JOURNAL OF GEOPHYSICAL RESEARCH, VOL. 102, NO. B7, PAGES 15,345–15,365, JULY 10, 1997

Natural gas hydrates on the southeast U.S. margin: Constraints from full waveform and travel time inversions of wide-angle seismic data

J. Korenaga[1] and W. S. Holbrook

Department of Geology and Geophysics, Woods Hole Oceanographic Institution, Woods Hole, Massachusetts

S. C. Singh and T. A. Minshull

Bullard Laboratories, University of Cambridge, Cambridge, England

Abstract. Strong bottom-simulating reflectors (BSR) have been mapped over a region of approximately 50,000 km^2 on the southeastern U.S. margin and have been associated with possible abundance of natural gas hydrates. In June 1992, coincident single-channel seismic and wide-angle ocean bottom seismic data were acquired in the region, focusing on the Blake Ridge and the Carolina Rise. Wide-angle reflections from the BSRs were clearly observed at offsets up to ~6 km. Joint travel time inversion was conducted with wide-angle and vertical-incidence data in order to explore possible regional variation, and the resultant two-dimensional average velocity models imply higher background velocities on the Carolina Rise. Full waveform inversion was then performed to determine the seismic origin of the BSRs. The best fit model shows a similar low velocity (~1.4 km/s) beneath the BSR at both sites, indicating trapped free gas with low saturation (<10%). The inversion results also indicate that a thin, high-velocity wedge, with a maximum velocity of ~2.3 km/s, is present just above the Blake Ridge BSR. Sediment reflectivities were also calculated, and higher reflectivities are observed on the Carolina Rise. An increase in reflectivity below the BSR seems to correspond to the gas-bearing zone at both sites. Concentration of hydrates were estimated based on these velocity models. Whereas average hydrate concentration of 3% of the total sediment volume is suggested for the lower half of the hydrate stability zone at the Blake Ridge, only a very low average concentration of hydrate can be expected at the Carolina Rise. The hydrates seem to be concentrated near the base of the hydrate stability zone, and the maximum hydrate concentration is estimated as ~20% at the Blake Ridge and ~7% at the Carolina Rise, both of which are too high to be explained by in situ biogenic activity only and require some secondary accumulation mechanism. It is suggested that hydrate recycling caused by the stability field migration may have effectively condensed hydrates at both sites. Additional enhancement by upward fluid expulsion may also be viable for the Blake Ridge.

Introduction

Gas hydrates are naturally occurring solids in which molecules of natural gas, mainly methane, are trapped in a lattice framework of water molecules [*Sloan*, 1990]. A mixture of water and methane can form gas hydrates at appropriate pressure and temperature conditions, which occur in marine sediment at water depths greater than a few hundred meters. The gas hydrate stability zone is limited to the upper hundreds of meters of the sediment section, below which temperatures are too high for hydrate to exist. Theoretically, a cubic meter of gas hydrate yields 164 m^3 of gas and 0.8 m^3 of water at standard temperature and pressure. This gas volume requirement restricts the occurrence of gas hydrates to continental margins, where biogenic methane production from organic-rich sediments is expected. Though thermogenic methane has been identified in sampled gas hydrates, its concentration is usually very low (less than a few percent) [*Kvenvolden*, 1993].

Methane gas trapped in gas hydrates may be economically important [*Kvenvolden*, 1988a; *MacDonald*, 1990], and because methane is a greenhouse gas, hydrates may have a major impact on the global climate system [*Kvenvolden*, 1988b; *Nisbet*, 1990; *Leggett*, 1990; *Paull et al.*, 1991]. Although accurate estimation of the global amount of methane stored in hydrates is essential for understanding these issues, so far proposed estimates differ by as much as two orders

[1]Also at MIT/WHOI Joint Program, Massachusetts Institute of Technology, Cambridge.

Paper number 97JB00725.
0148-0227/97/97JB-00725$09.00

of magnitude [*Dobrynin et al.*, 1981; *McIver*, 1981; *Kvenvolden*, 1988b; *Sloan*, 1990]. These estimates rely on the assumption of in situ conditions and thermodynamic state, and more realistic and quantitative estimation requires improved knowledge of actual hydrate distribution in marine sediments.

Velocity information provided by seismic experiments has been useful to infer possible hydrate distribution because pure hydrates have much higher velocity (3.3-3.8 km/s) [*Whalley*, 1980; *Sloan*, 1990] than normal sediments at depths of the hydrate stability zone. The base of the hydrate stability zone is often marked by a very strong reflector called a bottom-simulating reflector (BSR), and seismic characteristics of BSRs have been studied by many workers to investigate hydrate and free gas distribution near the base of the stability zone [e.g., *Minshull and White*, 1989; *Hyndman and Spence*, 1992; *Singh et al.*, 1993; *Katzman et al.*, 1994]. On the Atlantic continental margin, sediments above BSR sometimes show reduced reflectivities [e.g., *Paull and Dillon*, 198], and this "amplitude blanking" has also been associated with the presence of hydrates [e.g., *Dillon et al.*, 1993].

The purpose of this study is to investigate the hydrate distribution on the southeast U.S. margin, especially the Blake Ridge and the Carolina Rise, using wide-angle and vertical-incidence seismic data. Joint inversion of vertical-incidence and wide-angle travel times is performed to model two-dimensional (2-D) velocity structure. Full waveform inversion of wide-angle reflection data is then applied for nearly one-dimensional experiments to derive fine-scale velocity structure. Reflectivity analysis of vertical-incidence data is also conducted to quantitatively evaluate the amplitude blanking effect above BSR. Possible controlling factors for hydrate generation on the passive margin are discussed based on the comparison between the results from the two sites.

Data Description

The seismic data used in this study were acquired in June 1992 aboard R/V *Cape Hatteras* in a region where strong BSRs were mapped by previous studies [e.g., *Paull and Dillon*, 1981]. Single-channel seismic (SCS) profiling was conducted using a 160-cubic inch single air gun fired every 30 m, and wide-angle data were recorded coincidently on Woods Hole Oceanographic Institution ocean bottom hydrophones (OBH). Three SCS/OBH experiments were designed, two on the Blake Ridge and one on the Carolina Rise, and we present results from two experiments, one on each site. The Blake Ridge data have already been presented by *Katzman et al.* [1994] but are briefly reviewed here for completeness.

The Blake Ridge experiment is composed of a long dip line across the ridge flank (line 31) and two strike lines parallel to the ridge (lines 33 and 36). Four OBHs were deployed along the dip line, two of which also record the strike lines (Figure 1c). A very strong BSR is seen below OBH 19 in the SCS data. Amplitude blanking above the BSR is intense, and the blanking effect is prominent throughout the section even where no clear BSR is observed (e.g., below OBH 16, Figure 2a). *Katzman et al.* [1994] used the wide-angle data on the southeast part of line 33 for amplitude-versus-offset (AVO) analysis. Unfortunately, data on this line lack small offsets (< 0.5 km), which are crucial for successful τ-p transform [*Kappus et al.*, 1990]. For waveform inversion, we instead use the southwest part of line 31 (Figure 3a), where

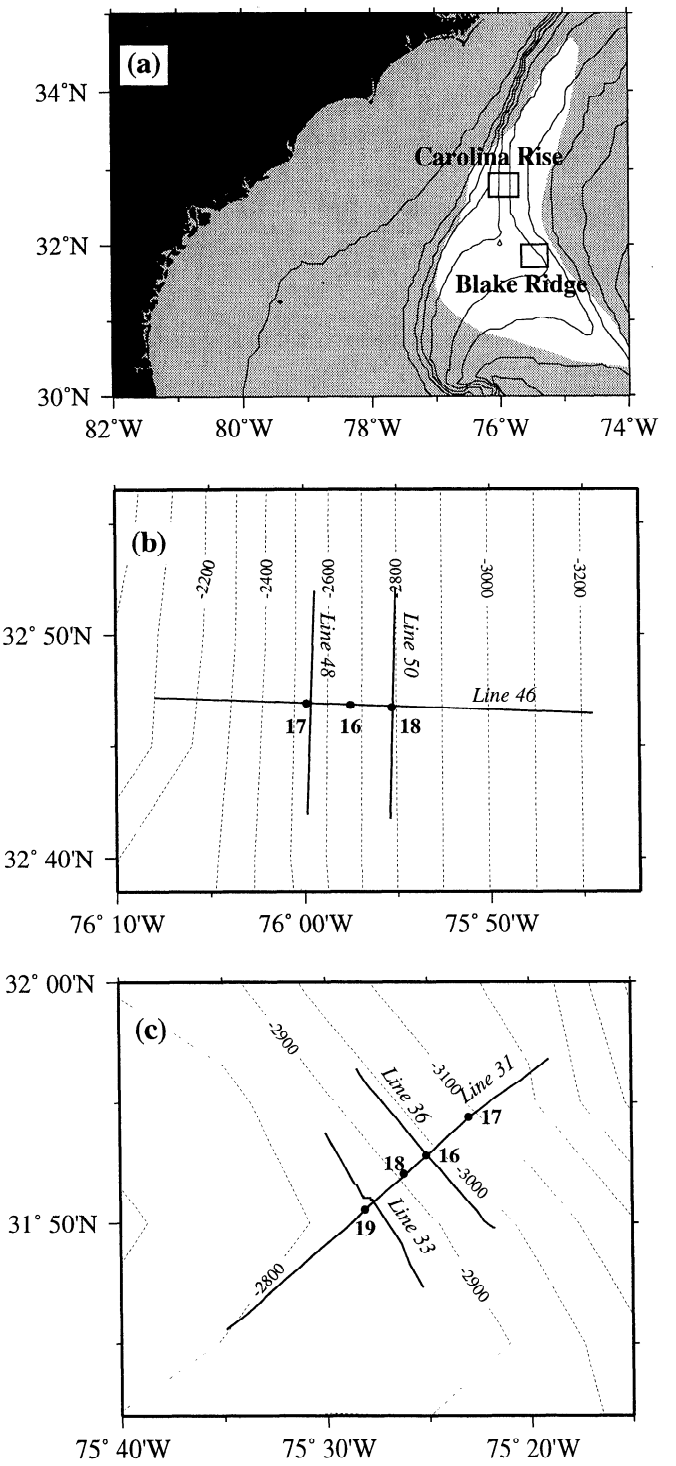

Figure 1. (a) Location map of surveyed area. The white region shows the extent of bottom simulating reflectors (BSR) from *Paull and Dillon* [1981]. Also shown are track lines of wide-angle ocean bottom seismic experiments on (b) the Carolina Rise and (c) the Blake Ridge. Solid circles show the location of ocean bottom hydrophones (OBH). Bathymetric contours are drawn at 500-m intervals in Figure 1a and 100-m intervals in Figures 1b and 1c.

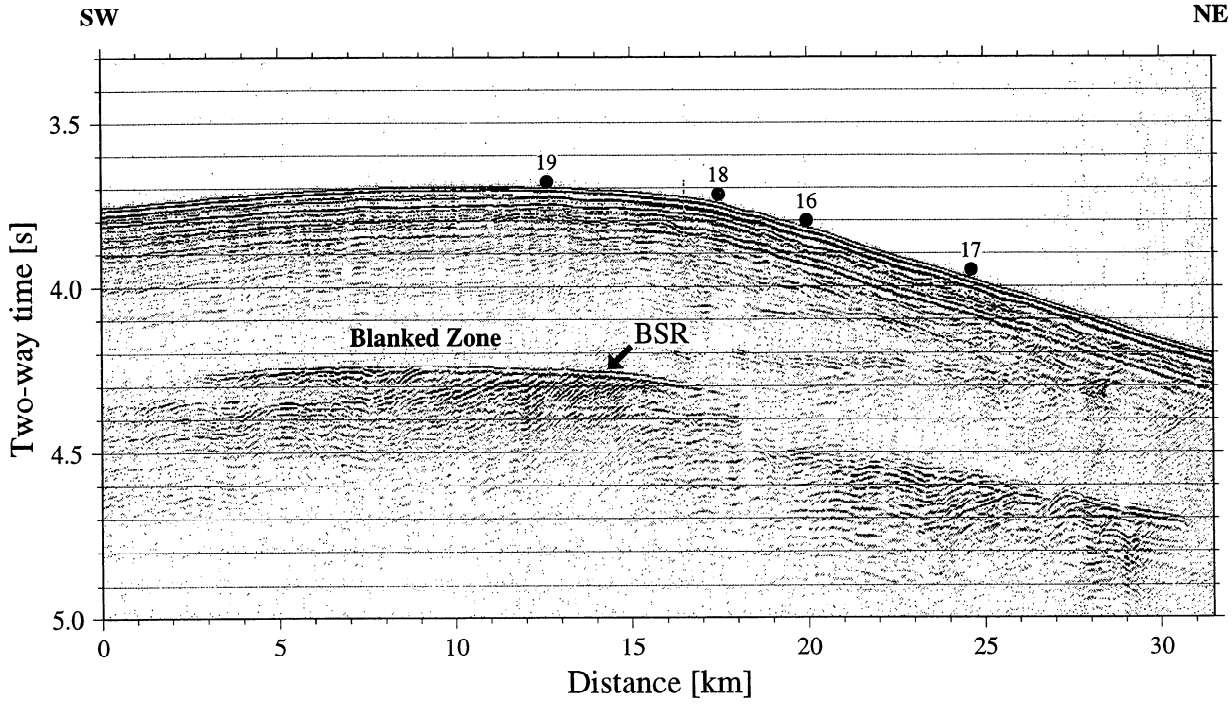

Figure 2a. Single-channel seismic (SCS) data from line 31, Blake Ridge. Data were band-pass filtered from 3 to 130 Hz, and a spherical divergence correction of $t^{1.0}$ was applied. Solid circles show the location of OBHs. The BSR is clearly seen below OBH 19, and the reflectivity above the BSR is remarkably low.

the seafloor and BSR are also almost flat (Figure 2a). A clear, large-amplitude BSR reflection can be traced up to the offset of ~6 km.

A similar survey line configuration was adapted with three OBHs in the Carolina Rise experiment (Figure 1b). A clear BSR is observed below OBH 18, and amplitude blanking is much less distinct than on the Blake Ridge (Figure 2b). The wide-angle data on the southern part of line 50 (Figure 3b), where the apparent dips of the seafloor and the BSR are less than 0.2°(Figure 2c), are used for waveform inversion. Another example of wide-angle data from line 46 is shown in Figure 3c. Although at least two phases between the direct

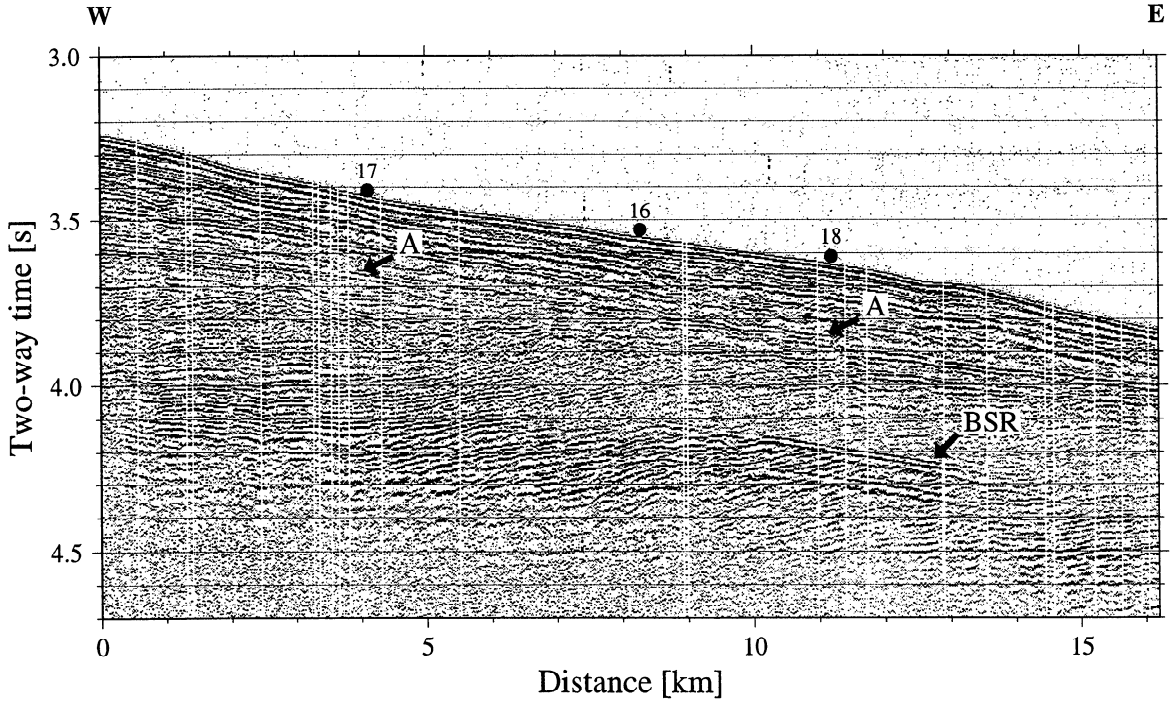

Figure 2b. SCS data from line 46, Carolina Rise. The BSR can be identified below OBH 18. Sedimentary strata seen below OBHs 16 and 17 seem to have relatively high reflectivity around 4.1-4.3 s. Phase A corresponds to the base of 1.65-1.68 km/s layer in Figure 4b.

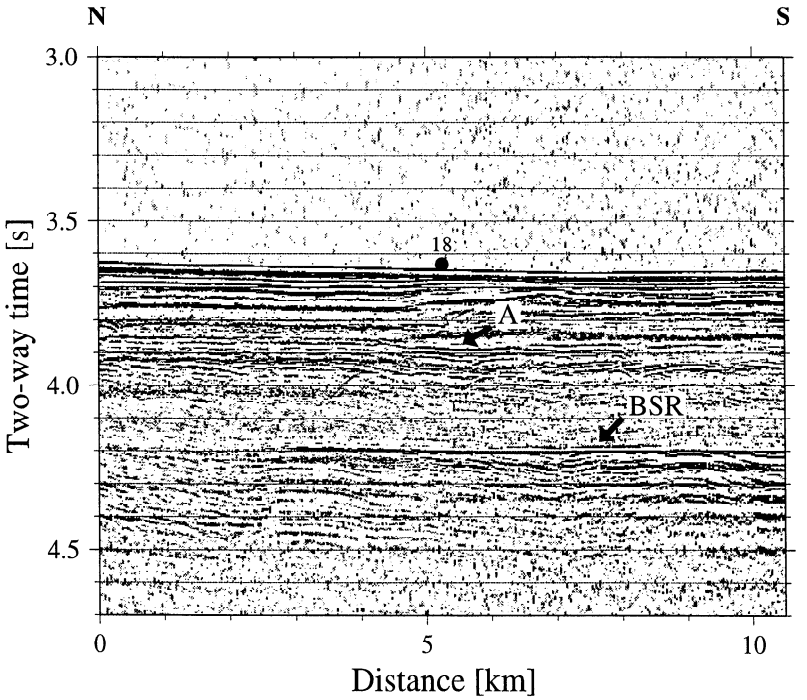

Figure 2c. SCS data from line 50, Carolina Rise. Seafloor is almost horizontal, and the BSR seems to be continuous over 5 km below OBH 18. Phase A corresponds to the base of 1.65 km/s layer in Figure 4c.

wave and the BSR reflection can be identified in most of wide-angle data sets, only one of them (labeled as phase A) is consistently traced for all data sets, and it is used for travel time analysis to constrain 2-D velocity structure above the BSR. Since the seismic source generated by the single air gun can be considered as a point source and each OBH is a single receiver, no source- or receiver-directivity correction is required for the wide-angle data sets used for waveform inversion.

Travel Time Inversion

In order to explore possible lateral variation in sediment velocities, a 2-D inversion was performed using the travel times of the wide-angle and vertical-incidence reflections. The SCS vertical-incidence data provide no constraints on velocities, but their spatially dense sampling supplies clear structural information. In conjunction with the structural constraints, the OBH wide-angle data are inverted to construct an accurate 2-D velocity model. Although the vertical spatial resolution expected from the travel time inversion is not as high as that obtained by the waveform inversion, average velocities above the BSR are still useful to estimate the bulk amount of hydrates within the hydrate stability zone. A 2-D velocity model for the Blake Ridge was derived by *Katzman et al.* [1994] (Figure 4a). The Carolina Rise data sets are analyzed here with the same method. First, the primary and multiple reflections in the wide-angle data are identified, and the corresponding phases in the SCS data are also identified. The travel times of the wide-angle and vertical-incidence phases are then digitized, and a velocity model that can simultaneously satisfy both travel times is constructed using an iterative, damped least squares inversion [*Zelt and Smith*, 1992].

There is strong lateral variation in the appearance of the BSR on line 46 (Figure 2b). The clear BSR is seen only below OBH 18 in the SCS data, and the reflection from the BSR is identified in the data of OBHs 16 and 18. Phase C in the OBH 17 data (Figure 3c), which looks similar to the BSR phase, is a reflection from one of the nearly horizontally layered reflectors, which are seen below OBH 17 at ~4.1 s in the SCS data. Phase C has a negative polarity as seen in the BSR phase, so its relatively strong amplitude may be associated with the presence of trapped free gas below the reflector. Phase A, a reflection from the middle of the hydrate stability zone, can be traced in all the OBH data sets, so two layers are introduced above the BSR. It is difficult to use more than two layers above the BSR; shallow reflectors are hard to identify in the wide-angle data because of the bubble pulse, and the correlation with the SCS data is often questionable. Increasing the number of layers also results in larger uncertainty in velocity estimation. A deeper reflection from below the BSR is vaguely identified in the wide-angle data at ~1 s after the BSR phase, and it is used for a very crude estimate of the velocity below the BSR, averaging over a depth of more than 1 km. Therefore three layers in total are introduced below OBH 18, and four layers are introduced below OBH 17. Since there is no BSR evident below OBH 17, no velocity contrast is allowed between the second and the third layers there during the inversion.

We first inverted for the two strike lines, lines 48 and 50, which have nearly 1-D structure, and used the results to construct a starting model for line 46 by fixing depths and velocities at the two intersections. We tried to optimize the number and location of depth and velocity parameters so as to keep high resolution of all parameters; parameter resolution values calculated from the inversion ensure that the models are not overparametarized [*Zelt and Smith*, 1992].

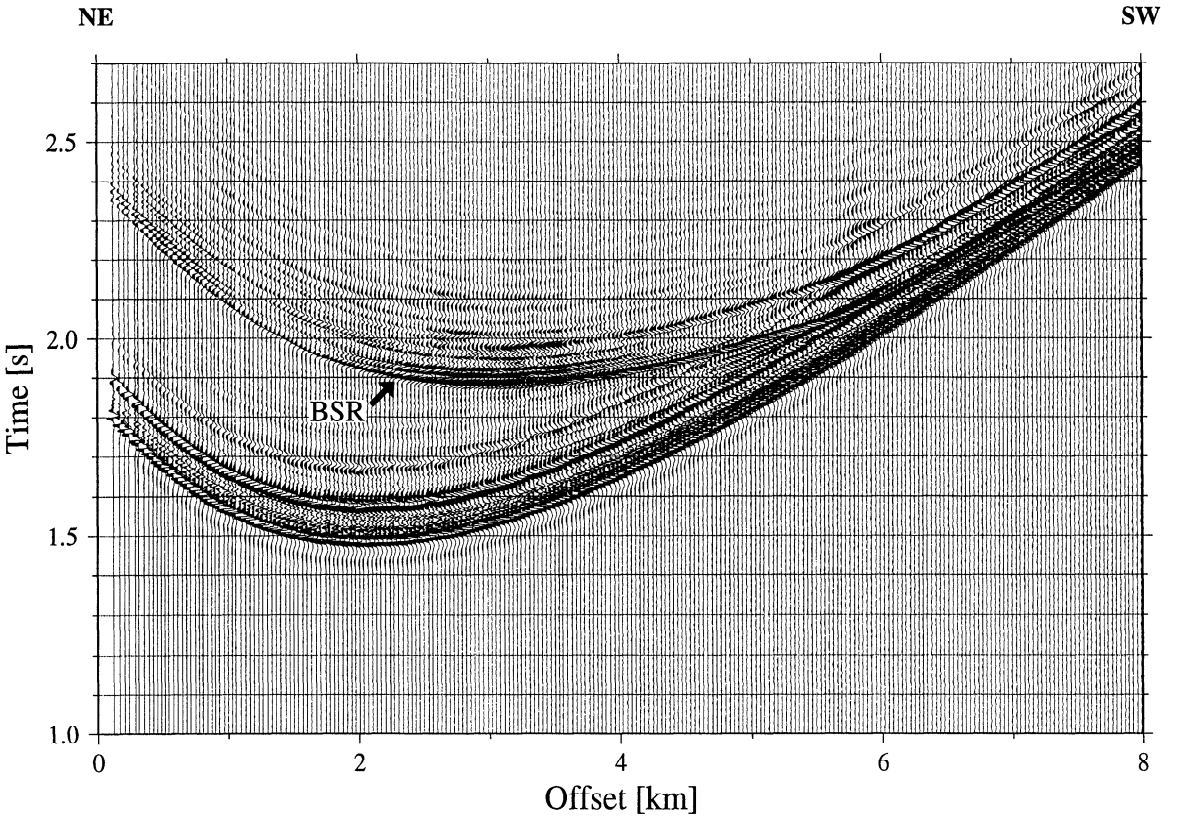

Figure 3a. Blake Ridge wide-angle data from OBH 19, line 31, to the southwest, plotted with reduction velocity of 2.5 km/s. Data were processed with high-pass filter of >25 Hz and a spherical divergence correction. The BSR phase is clearly observed at offsets up to ~6 km.

The resultant velocity models for lines 46 and 50 are shown in Figures 4b and 4c.

In order to estimate uncertainty in the solution, we performed a sensitivity analysis by perturbing velocity parameters. The 2-D travel time inversion is a more complicated problem than 1-D inversion, and there has been no definite method to evaluate the uncertainty; a slight change in the dip of a reflector, for example, results in different ray coverage, and the correspondence between model parameters and travel time data is highly complex. Here we choose the RMS travel time residual as a reasonable guideline. We perturb a certain parameter, hold it fixed, and invert for the rest of the parameters. The RMS travel time residual increases as the perturbation becomes larger, and an error bound is determined where model travel time misfits exceed the travel time pick error (0.01 s) over 1/3 of the data. An error bound of 0.06 km/s, similar to that estimated by *Katzman et al.* [1994] (0.05 km/s), is obtained for both the first and the second layers (Figure 5).

For the first layer beneath the seafloor, the Carolina Rise model shows higher velocities (1.65-1.68 km/s) than the Blake Ridge model (1.58 km/s), which suggests that sediments are more consolidated at the Carolina Rise or that sedimentary matrix velocities at the Carolina Rise are higher or both. The velocities immediately above the clear BSRs are, however, nearly equal at the Blake Ridge and the Carolina Rise considering the estimated error bounds. The higher average velocity below OBH 17 (1.95 km/s) probably resulted from the larger layer thickness; the velocity of the second layer below OBH 17 can be similar to that below OBH 18 if the velocity of the third layer is as high as ~2.1 km/s.

Waveform Inversion

In order to resolve finer-scale velocity structure around BSR, 1-D waveform inversion is applied to the OBH 19 data on line 31 (Blake Ridge) and the OBH 18 data on line 50 (Carolina Rise). Waveform inversion employs the minimization of the difference (misfit) between observed seismogram and synthetic seismogram. Complete synthetic seismograms are computed using the generalized reflection transmission matrix method [*Kennett and Kerry*, 1979], and the misfits are calculated in the frequency-slowness (ω-p) domain. A τ-p transform followed by a Fourier transform thus needs to be applied to the observed time-offset (t-x) data, prior to the inversion. The misfit function to be minimized is highly nonlinear and thus requires a Monte Carlo random search to confirm that a global minimum is found. However, a random search is very time consuming when the number of model parameters is large, so our inversion strategy consists of the following two steps: (1) the construction of a background velocity model (long-wavelength velocity variation) based on the prior travel time inversion, and (2) a local search to estimate short-wavelength velocity variation [*Kormendi and Dietrich*, 1991].

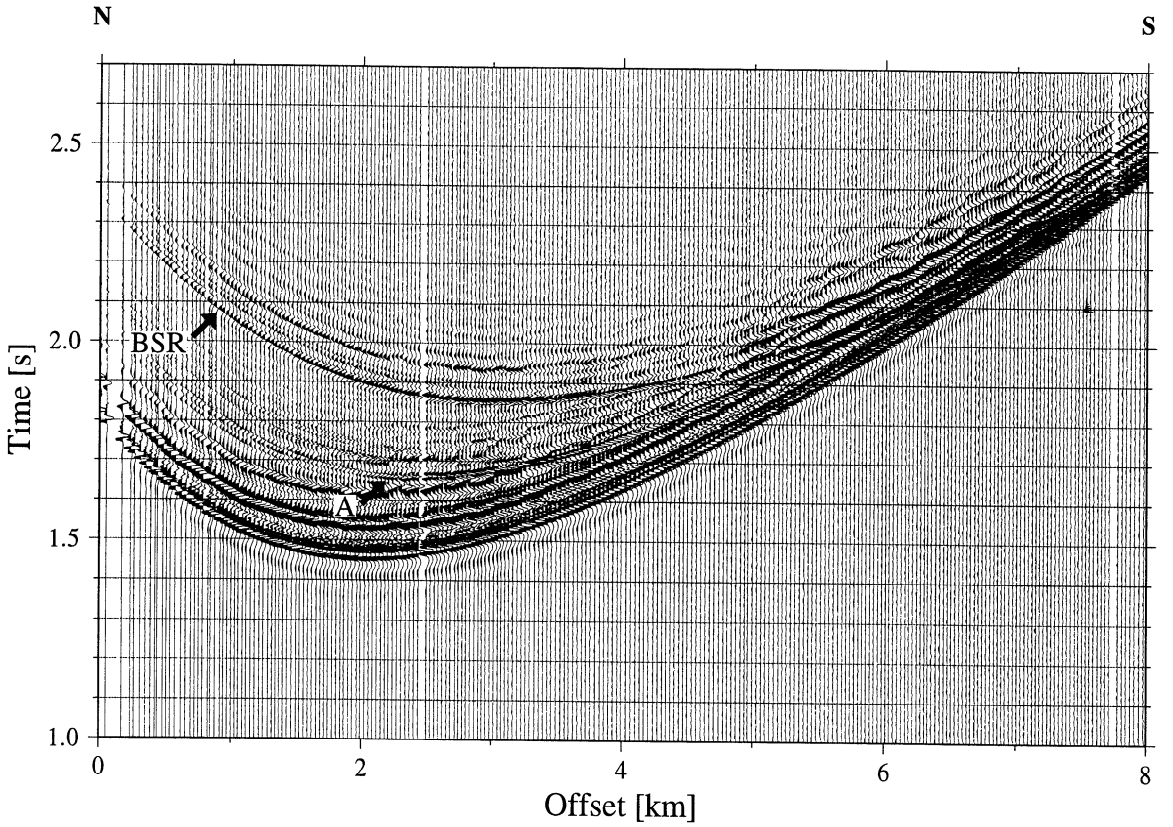

Figure 3b. Carolina Rise wide-angle data from OBH 18, line 50, to the south. Phase A corresponds to the base of 1.65 km/s layer in Figure 4c.

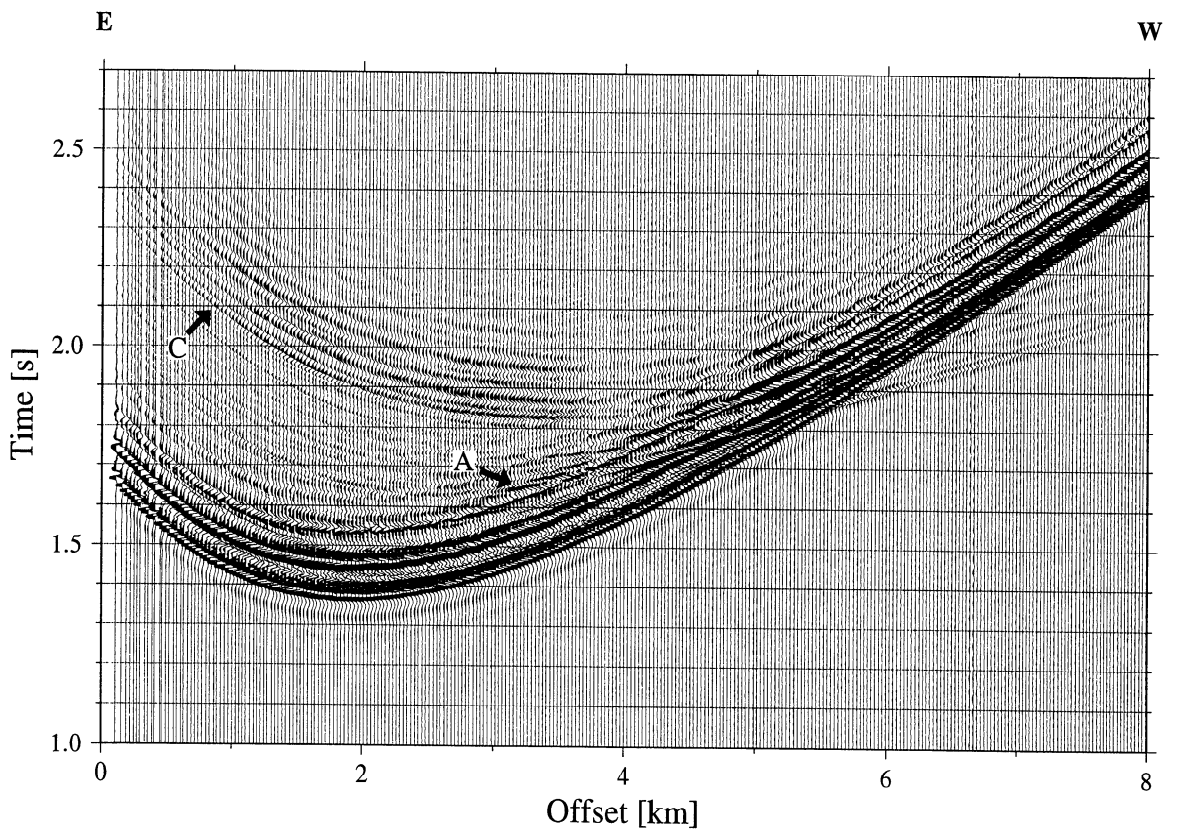

Figure 3c. Carolina Rise wide-angle data from OBH 17, line 46, to the west. Phase C corresponds to the base of 1.95 km/s layer in Figure 4b, showing negative polarity like BSR phase.

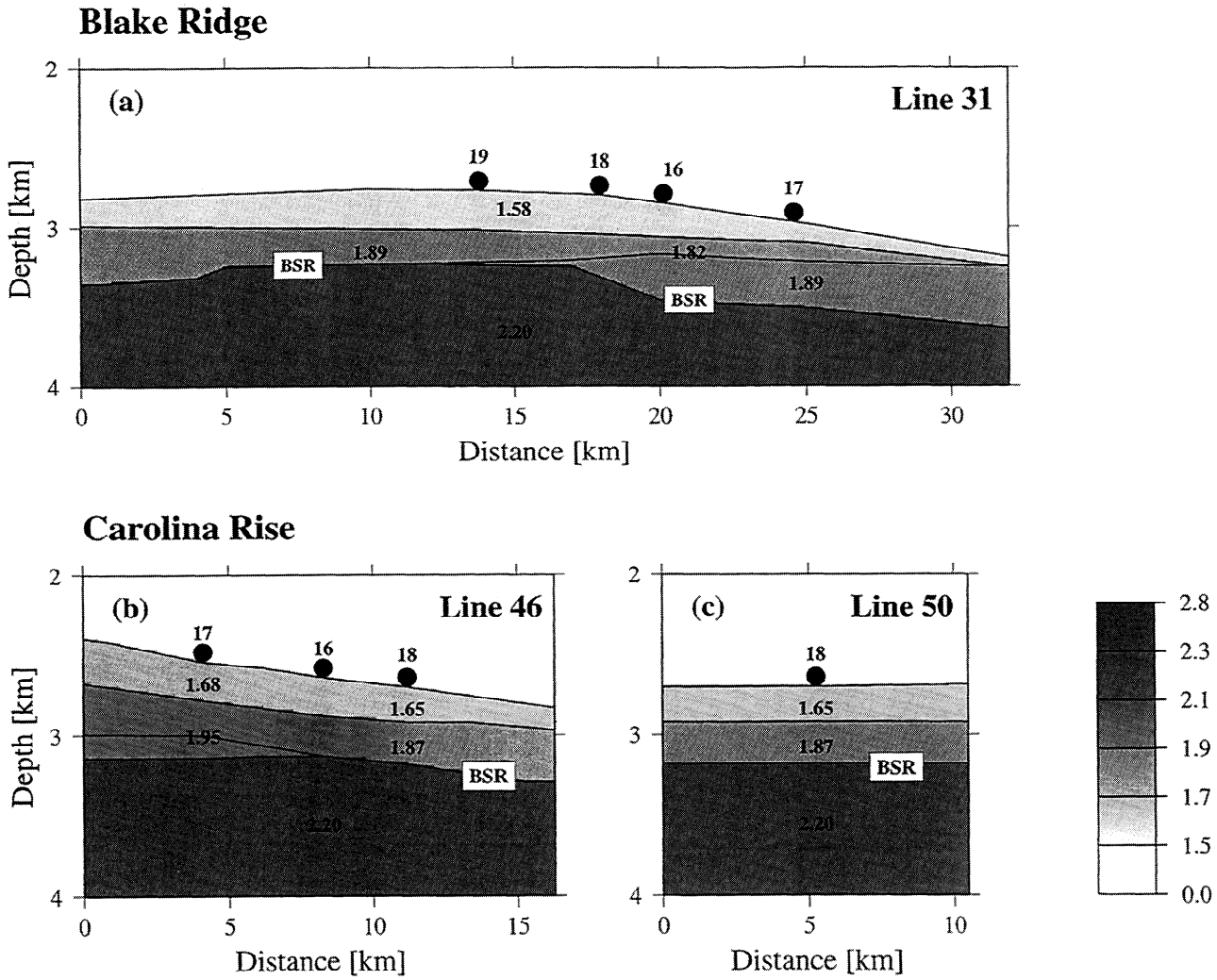

Figure 4. Two-dimensional average velocity models from travel time inversion for (a) Blake Ridge [after *Katzman et al.*, 1994] and (b) and (c) Carolina Rise. Velocities are labeled in kilometers per second, and shading is proportional to velocity. Solid circles mark the location of OBHs.

The τ-p Transform

The delay time-slowness (τ-p) mapping of seismic data is particularly useful for 1-D seismic analysis since it decomposes the medium response into a series of non-interacting cylindrical waves. The τ-p transform appropriate for a point source or 3-D geometry may be accomplished by the following successive transformations [*Harding*, 1985]:

Fourier transform

$$\hat{u}(\omega, x) = \int_{-\infty}^{\infty} u(t, x) \exp(i\omega t) dt \qquad (1)$$

Hankel transform

$$\hat{u}(\omega, p) = \int_{0}^{\infty} x J_0(\omega p x) \hat{u}(\omega, x) dx \qquad (2)$$

where J_0 is the zero-order Bessel function.
Inverse Fourier transform

$$u(\tau, p) = \frac{1}{2\pi} \int_{-\infty}^{\infty} \hat{u}(\omega, p) \exp(-i\omega\tau) d\omega \qquad (3)$$

Another method of 3-D τ-p transformation proposed by *Henry et al.* [1991], which is based on linear inversion theory, cannot be implemented with most of the artifact removal methods described below. The 2-D [*Schultz and Claerbout*, 1978] and 2-D+ [*Chapman*, 1981] approximations provide much faster formulas, but their accuracy is insufficient for waveform inversion [*Kappus et al.*, 1990].

Incompleteness of field data can result in transform artifacts, which must be removed as much as possible for successful waveform inversion. Three major types of artifacts are identified: (1) truncation effect due to limited data extent in the t-x domain, (2) aliasing due to sparse sampling (mainly with respect to offset), and (3) pseudo-truncation effect due to inconsistent gun signatures. The truncation effect can be alleviated by tapering prior to the Fourier transform (equation (1)): we applied a cosine taper for offset from 7.4 km to 8 km, and for time from 1.0 s to 1.2 s and from 4.8 s to 5.0 s. Two types of aliasing can occur in the 3-D τ-p transform with insufficient trace spacing: aliasing from positive slowness integral (occurring at small slownesses; we call this $+p$ aliasing hereafter) and aliasing from negative

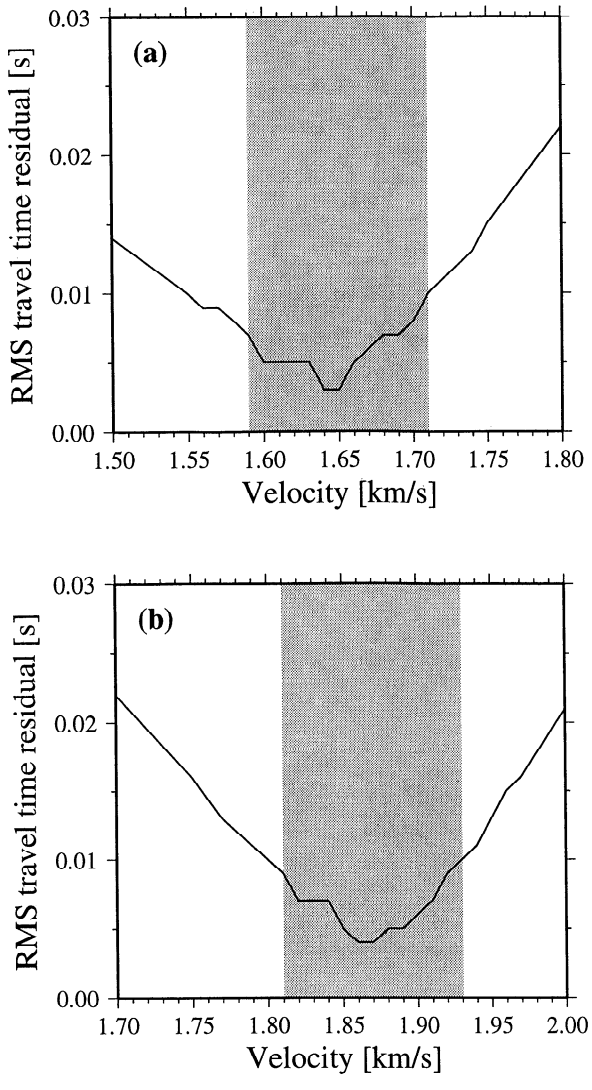

Figure 5. RMS travel time residual as a function of velocity (a) in the first layer and (b) in the second layer of the line 50 velocity model (Figure 4c). Shading shows estimated uncertainty of ±0.06 km/s.

slowness integral (occurring at large slownesses; -p aliasing) [*Harding*, 1985]. A weighting filter proposed by *Singh et al.* [1989] can reduce the +p aliasing if alignment slowness information is available. A simple velocity model obtained by primary travel time analysis is sufficient to supply this slowness information. The -p aliasing can be avoided if the Hankel function instead of the Bessel function is used for larger slownesses [*Harding*, 1985]; we used the Hankel function for the slownesses larger than 0.03 s/km.

Figure 6a shows the result of the τ-p transform of the Carolina Rise data with the above treatments. The waveform of the transformed BSR phase seems to change trace by trace in an inconsistent manner, and careful inspection of the original field data revealed that the BSR phase was distorted by linear artifacts originating in inconsistent gun signatures (pseudo-truncation effect). Because ocean bottom seismic data include direct waves whose amplitudes are much larger than subsequent reflections, even small inconsistencies could produce linear artifacts that may badly influence the transform of the subsequent reflections. In order to suppress the influence of the signature variation, we first tried trace-wise deconvolution in the t-x domain, which only deteriorated the situation because of deconvolution artifacts. We also tried the data windowing used by *Schultz and Claerbout* [1978] and found that simple windowing could not preserve data power correctly. A more sophisticated method was thus implemented with the primary velocity model, which was also used for the +p aliasing removal. The number of input (t-x) traces contributing to each output (τ-p) trace is related to the inverse curvature of the t-x curve $x'(p_0)$ as [*Harding*, 1985]

$$N_c \propto \left[\frac{x'(p_0)}{\omega \Delta x^2}\right]^{\frac{1}{2}} \tag{4}$$

where p_0, ω, and Δx are stacking slowness, frequency, and trace sampling interval, respectively, and

$$x'(p_0) = \left.\frac{dx(p)}{dp}\right|_{p=p_0}. \tag{5}$$

The effective window width ($\sim N_c \Delta x$) is thus proportional to the square-root of the inverse curvature scaled by frequency. The degree of contribution of an input datum with an offset of x and an alignment slowness of p_a, to the integral at the slowness p_0, can be measured with the following offset normalized by the effective window width:

$$\frac{x(p_a) - x(p_0)}{N_c \Delta x} \propto \sqrt{\frac{\omega}{x'(p_0)}}\, x'(p_0)(p_a - p_0) \tag{6}$$

because the alignment slowness can be approximated as

$$p_a \sim p_0 + x'(p_0)^{-1}(x(p_a) - x(p_0)) \tag{7}$$

using the first-order Taylor expansion. The primary velocity model is used to assign the curvature as well as the alignment slowness p_a to each input datum, and a weighting function is then constructed as

$$w(x,t) = \frac{S}{\sqrt{\omega_D x'(p_0)}|p_0 - p_a|}, \tag{8}$$

with the upper limit of unity, where S is an arbitrary scaling factor and ω_D is a dominant, representative frequency of input data. A smaller S corresponds to narrower windowing, and the smallest possible value of S with which most linear artifacts are removed while preserving the power of true phases must be determined empirically. For the dominant frequency of 45 Hz we found S of ~5 produced the best result (Figure 6b). The τ-p traces for small slowness (p < 0.03) are still noisy because random noise tends to be accumulated at these slownesses due to a less oscillatory Bessel function in the Hankel transform, and they are not used for the waveform inversion.

Long-Wavelength Velocity Estimation

In order to prepare background velocity models for waveform inversion, we repeated the travel time inversion for the two locations with slightly different conditions. The velocity at the seafloor was fixed at 1.5 km/s, which is a reasonable

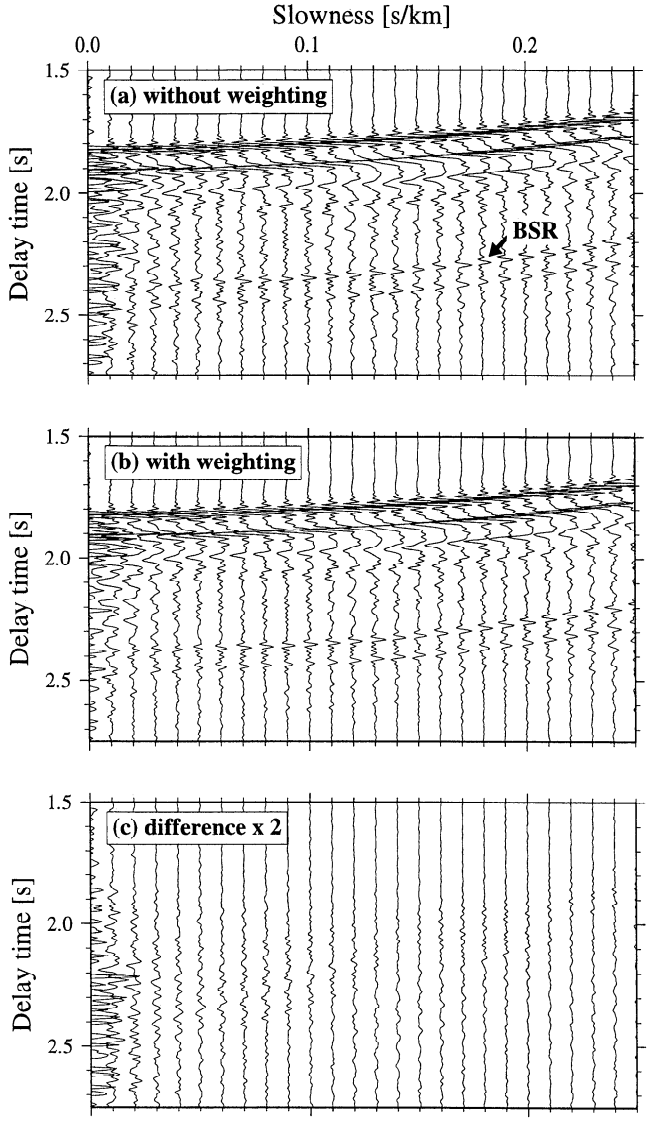

Figure 6. The τ-p transform of Carolina Rise data with artifact removal methods. (a) After alias removal, BSR phase still looks somewhat incoherent trace by trace. (b) Pseudo-truncation effect (c) is significantly reduced by weighting of equation (8).

assumption for the P wave velocity of the sediments just beneath the seafloor, and we first inverted for the velocity gradient and the depth of the first layer. The resultant gradients are 0.81 s^{-1} for the Blake Ridge and 1.23 s^{-1} for the Carolina Rise, and the predicted maximum offset for the reflection from the base of the layer well matches the observation. The velocity gradient of the second layer was then estimated as $\sim$0.5 s^{-1} at both locations, which corresponds to the observed maximum offset for the BSR reflections ($\sim$6 km).

A Monte Carlo search to maximize the semblance energy of major reflectors has been often used to estimate long-wavelength variation prior to waveform inversion [e.g., *Singh et al.*, 1993; *Minshull et al.*, 1994]. We also tried this approach and found that the resultant velocity for the second layer is lower than that by the travel time inversion by $\sim$0.05 km/s. This is because the travel time inversion uses the first-break time of the BSR reflection, while the random search uses the most dominant phase in the BSR reflection, which is most easily identified in the semblance calculation and comes slightly after the first break. Though the random search has the advantage of avoiding errors due to layer stripping, we adapt the long-wavelength velocity models derived from the above travel time inversion; it is the first-break travel time that must be reproduced by the model, and the advantage of the random search seems to be less significant when only two layers are introduced above BSR.

Short-Wavelength Velocity Estimation

Starting from the long-wavelength velocity model, a local search using the conjugate gradient method is performed to derive short-wavelength structure [*Kormendi and Dietrich*, 1991]. The misfit function is defined as

$$S(\boldsymbol{m}) = \frac{1}{2}(||\boldsymbol{d}_{\text{cal}} - \boldsymbol{d}_{\text{obs}}||_D^2 + ||\boldsymbol{m} - \boldsymbol{m}_0||_M^2) \qquad (9)$$

where $\boldsymbol{d}_{\text{cal}}$ is the calculated wave field corresponding to the model $\boldsymbol{m}$, $\boldsymbol{d}_{\text{obs}}$ is the observed wave field, and $\boldsymbol{m}_0$ is the initial model. The norms $||\ ||_D^2$ and $||\ ||_M^2$ are L_2 norms weighted by the data covariance matrix C_D and the model covariance matrix C_M, respectively. We tested several different combinations of C_D and C_M, ranging from $C_M = 0.1I$ to $C_M = 10I$ with fixing $C_M = 1.0I$, in order to find a reasonable pair of covariance matrices, with which stable model evolution can be obtained. C_D and C_M were set as $1.0I$ and $2.0I$ in the following inversion, but changing these values by a small factor would produce the almost same results. The partial derivatives with respect to model parameters are calculated from an analytical solution [*Dietrich and Kormendi*, 1990] to construct the conjugate gradients. The model parameters include P and S wave velocities, density, and P and S wave attenuations as functions of depth, and a simultaneous inversion for P and S wave velocities and density is theoretically possible [*Kormendi and Dietrich*, 1991]. Because we do not have good starting models for S wave velocity and density, however, only P wave velocities are updated by the conjugate gradient search. Other elastic parameters are assumed as described below and are fixed during the inversion.

The background velocity models obtained in the previous step must be smoothed to avoid large discontinuities at the reflectors, which would introduce high-amplitude and high-frequency energy to synthetic seismograms thereby destabilizing the inversion. Since we do not have a good estimate for the interval velocity beneath the BSR, the velocity of the base of the second layer (1.97 km/s for Blake Ridge and 1.94 km/s for Carolina Rise) was continuously used for the deeper section. Other possible choices include to keep the same velocity gradient (0.5 s^{-1}) and to specify some lower velocity below the BSR, but we prefer to use the constant velocity continuation as a neutral choice. The models were then discretized at 5-m intervals and smoothed with a triangular average filter of 40-m window width. From the P wave velocities, S wave velocities and densities were calculated using the empirical relations by *Castagna et al.* [1985] and by *Hamilton* [1978], respectively. Sediment Q values were set at 200 for P waves and 100 for S waves [*Minshull and Singh*, 1993]. Finally, the densities at the seafloor were mod-

ified to reproduce the seafloor reflection coefficients (0.176 for the Blake Ridge and 0.199 for the Carolina Rise), which were determined from the amplitudes of the first arrival and the first multiple.

The source wavelet used for the inversion was deconvolved from the first multiple with the first arrival. The OBH is located on the seafloor, and the first arrival on the OBH is thus a combination of the direct wave and the seafloor reflection. After a spherical divergence correction, the first arrival (P) and the first multiple (M) at vertical incidence for the OBH geometry may be expressed as

$$P(t+T_{sf}) = (\delta(t)+r(t)) * s(t) \quad (10)$$

$$M(t+3T_{sf}) = -(\delta(t)+r(t)) * r(t) * s(t) \quad (11)$$

where T_{sf} is one-way travel time from the sea surface to the seafloor, $\delta(t)$ is the delta function, $r(t)$ is a seafloor response function, s(t) is a source wavelet, and asterisk is the convolution operator. Therefore the source wavelet can be determined by successive deconvolution as

$$r(t) = -M(t+3T_{sf})/P(t+T_{sf}) \quad (12)$$

$$s(t) = P(t+T_{sf})/(\delta(t)+r(t)) \quad (13)$$

where slash is the deconvolution operator. Results from several near-vertical-incidence traces ($x < 200$ m) were stacked to increase the signal-to-noise ratio (Figure 7). The estimated source wavelet closely resembles the first arrival. The difference between the source wavelet using only one trace and the stacked source wavelet is much smaller than the dominant waveform, indicating reliable source wavelet estimation. The length of the source wavelet is ~0.4 s to include up to the third bubble pulse.

If the source wavelet is scaled to a peak-to-peak amplitude of 1.0, the data must be scaled so that the peak-to-peak amplitude of the first arrival (direct wave and seafloor reflection) at vertical incidence matches $1.0+R_{sf}$, where R_{sf} is the seafloor reflection coefficient. Since the contribution of R_{sf} to the scaling is small ($R_{sf} \sim 0.2$), careful data scaling is required to correctly derive the subbottom impedance contrasts by waveform fit. We calculated a single scaling factor to apply to all τ-p traces by the following method. First, a scaling factor C for each τ-p trace was calculated to minimize the following misfit:

$$\Delta = \sum_{i=1}^{N_t} [S(p,\tau_i) - C(p)D(p,\tau_i)]^2 \quad (14)$$

where D is the data, S is the synthetics, and N_t is the number of samples in the time series, and thus $C(p)$ was given by

$$C(p) = \frac{\sum_{i=1}^{N_t} D(p,\tau_i)S(p,\tau_i)}{\sum_{i=1}^{N_t} D(p,\tau_i)^2}. \quad (15)$$

Then, traces for which $C(p)$ differed from the average by more than 5% were rejected, and the final scaling factor was determined by averaging the factors of the remaining traces. Although the S wave velocity at the seafloor is important for the seafloor reflection coefficient at large slowness, a possible error in the empirical estimate of the S wave velocity has only negligible influence on this approach. The resultant Blake Ridge data have the slowness range of 0.07-0.50 s/km, and the Carolina Rise data have the range of 0.06-0.49 s/km. The missing energy at discarded slownesses results from residual artifacts at the smaller slownesses and from the limited offset range at the larger slownesses. The constant scaling factor for the wide slowness range indicates that the assumption of no receiver and source directivities is reasonable.

The waveform inversion consisted of five runs, and the final result of each run served as the starting model $\boldsymbol{m}_0$ for the next run. The successive runs used increasing ranges of frequency and slowness, and the final run used the full slowness range and a frequency range of 10-50 Hz. The subbottom velocity structure was represented by the stack of 5-m-thick homogeneous layers. The thickness of 5 m was so chosen to be less than one-fifth of a wavelength for the dominant frequencies, which is required for the precise computation of the synthetics [*Chapman and Orcutt*, 1985]. Because a small error in the source wavelet estimation can result in a spurious velocity variation near the seafloor, the first 20 velocity parameters were fixed throughout the inversion. This strong preconditioning hardly affects the short-wavelength velocity structure near the BSR, which is influenced mainly by the waveform of the BSR phase [*Jannane et al.*, 1989].

The final results of the inversion for the Blake Ridge and Carolina Rise data are shown in Figure 8. The velocity structure around the BSR is very different between the two sites. For the Blake Ridge data, a gradual increase in velocity up to ~2.3 km/s followed by a sharp drop to 1.4 km/s was derived to reproduce the BSR waveforms. The Carolina Rise result shows a similar velocity drop beneath the BSR

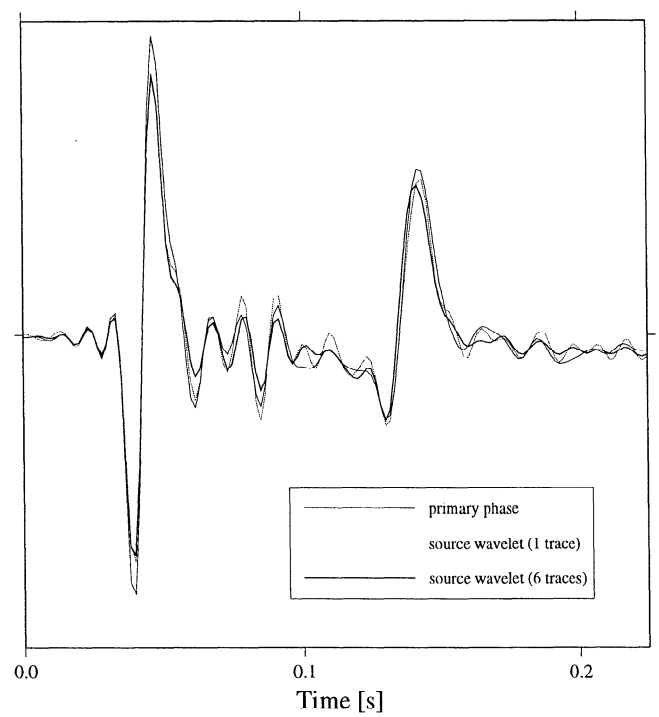

Figure 7. Example of source wavelet estimation (Blake Ridge). Thin line shows the first arrival that includes direct wave and seafloor reflection. Dashed line is source wavelet estimated with one trace, and thick line is stacked wavelet using six traces.

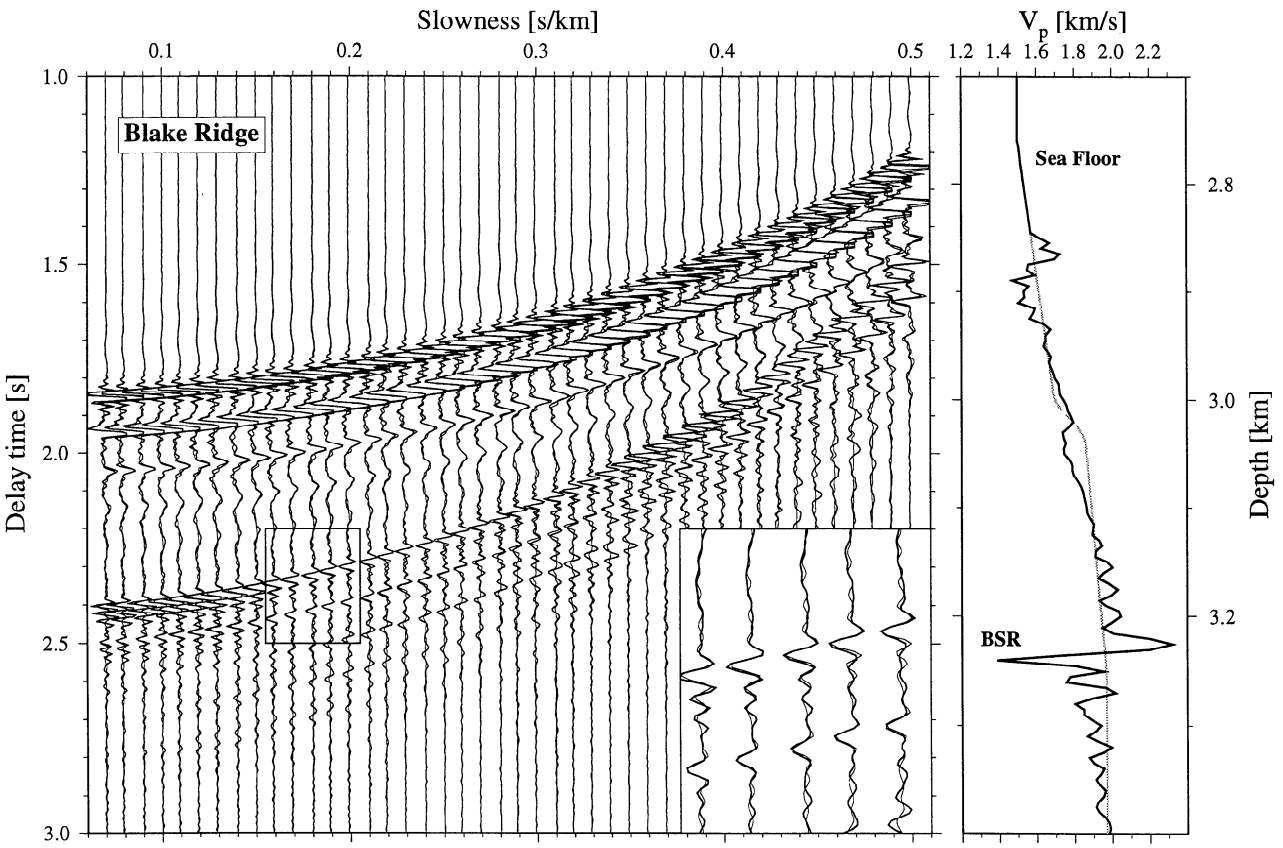

Figure 8a. Blake Ridge (OBH 19, line31) data in the τ-p domain (thick line), plotted with best fit seismogram (thin line). Frequency range is 10-50 Hz. Inset is enlargement of a portion of BSR phase, showing extremely good waveform agreement. Corresponding velocity model is shown to the right; gray line is starting long-wavelength velocity model. See text for details.

(~1.4 km/s) without a notable velocity increase above the BSR. Assuming that the velocity of the normal sediments at the depths of the BSR is 1.9 km/s, the velocity drop of 0.4-0.5 km/s probably corresponds to a gas-bearing zone beneath the BSR where the free gas saturation is less than 10% [*Domenico*, 1976; *Murphy*, 1984; *Ostrander*, 1984]. The thickness of the gas zone may be as large as 50 m at the Blake Ridge and ~10 m at the Carolina Rise. The velocity increase above the Blake Ridge BSR can be explained by the presence of hydrates; an estimate of the amount of hydrate is discussed later.

Excellent waveform fit is achieved throughout the entire slowness range for the Carolina Rise data. The waveform fit for the Blake Ridge data is slightly poorer for small (<0.15 s/km) and medium (0.35-0.40 s/km) slownesses, probably because of 2-D effects in the OBH geometry. The bottom point for the BSR reflection recorded by an OBH is not a common depth point; it spreads up to ~1 km for an offset of 6 km [*Katzman et al.*, 1994]. As seen in the Blake Ridge SCS profile, sedimentary strata cut across the BSR below OBH 19, possibly resulting in the above noted poor fits. Because the waveform inversion is constrained by all slownesses, the waveform variation due to the 2-D effect tends to be smoothed out rather than badly influence the inversion, and the resultant velocity model may be regarded as an averaged 1-D structure.

Reliability of Inversion Solution

For a quantitative comparison of the results, it is important to inspect the reliability of each result. In particular, the Blake Ridge velocity model shows more complex structure than the Carolina Rise model, so we investigated how the complex structure corresponds to the observed data. First, the oscillatory structure seen above and beneath the BSR is smoothed to evaluate the contribution of the reverberation caused by the fine-scale structure. The resultant synthetics still fit the data similarly well, except for high-frequency components (Figure 9b); the increase in the misfit is ~14%. The reverberation thus does not affect the dominant amplitudes. Since the high-frequency components following the main BSR phase are too large to be considered a part of the source wavelet (Figure 7), the short-wavelength variation around the BSR is not an artifact caused by error in the source wavelet estimation. The waveform fit for the high-frequency components by the best fit model is not consistently good for the whole slowness range, and we believe that the high-wavenumber oscillations resulted from forcing a 1-D inversion to the two-dimensional, fine-scale structure around the BSR. The low-velocity spikes below the BSR, for example, may be explained by free gas trapped by the crosscutting sedimentary strata beneath the BSR.

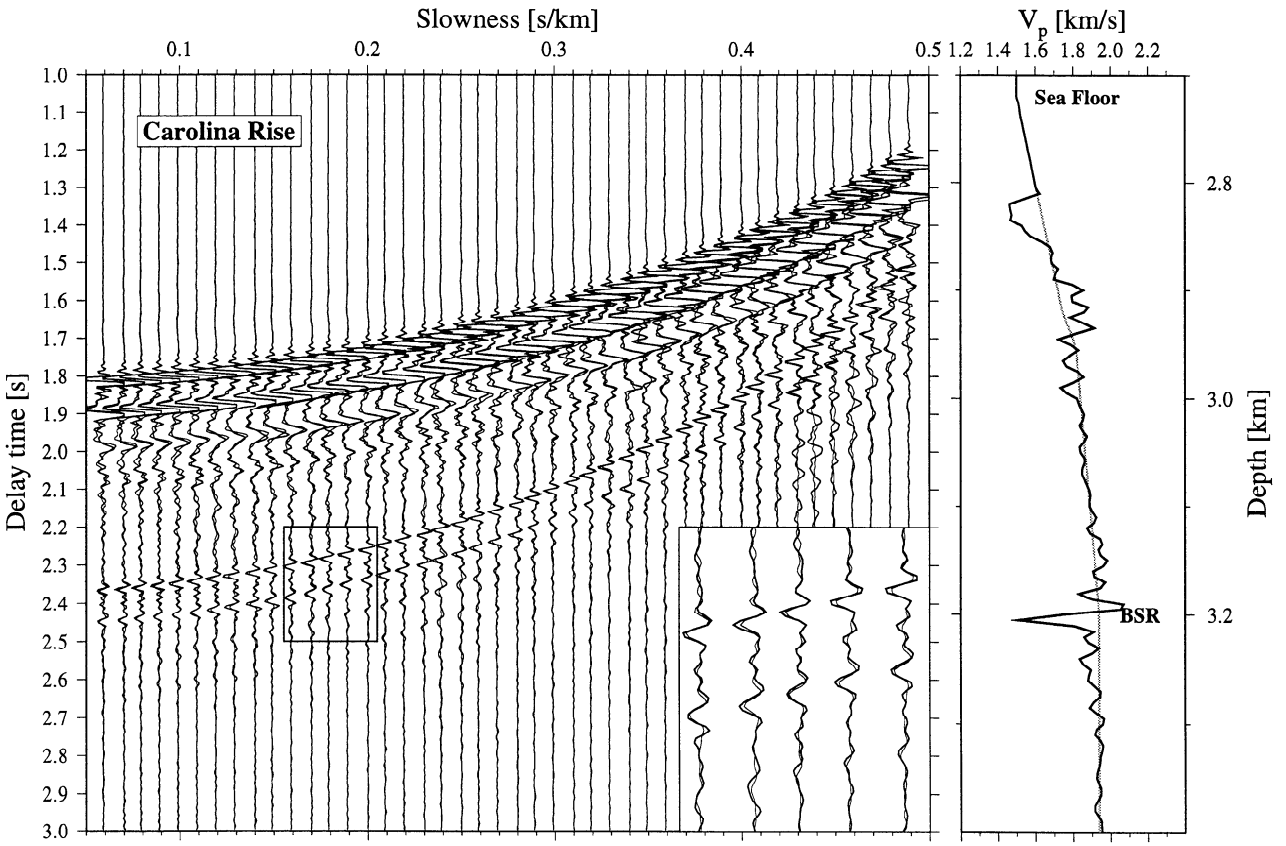

Figure 8b. Carolina Rise (OBH 18, line 50) data in the τ-p domain, plotted as Figure 8a. Remarkable waveform fit was achieved throughout the whole range of slownesses.

Next, we performed two inversions with different constraints to investigate the necessity of having both a high-velocity wedge and a low-velocity zone (LVZ) around the BSR. The first inversion used the smoothed velocity model (Figure 9b) as a starting model, except that velocities below 3.25 km were replaced with 1.97 km/s and fixed throughout the inversion. The high-velocity wedge grew to ~2.5 km/s, and the final misfit is only 14% higher than that of the best fit model. The resultant amplitude-versus-slowness behavior of the wedge-only synthetics is, however, very different from the observed one. The maximum positive amplitude of the BSR phase for this model is consistently larger than the maximum negative amplitude (Figure 10b), which is contrary to the observed pattern (Figure 10a) where the maximum negative amplitude is on average 2 times greater than the positive maximum amplitude over nearly the entire slowness range. In the second inversion, the maximum possible velocity was set at 1.97 km/s in order to test the possibility of LVZ-only models. The misfit of the final LVZ-only model is ~30% larger than that of the best fit model, and importantly, the modeled BSR waveforms produced by the LVZ are significantly phase-delayed with respect to the observed waveforms, which are nearly minimum phase (Figure 10c). Thus we conclude that both the high-velocity wedge and the LVZ are required to reproduce the observed waveforms.

The local search must start with a good initial model to converge into the global minimum. Since the number of reflectors used for the long-wavelength velocity variation may be too small to construct a sufficiently good starting model, the final result of the inversion may represent merely an example of local minima. Four candidate starting models were prepared for each data set to explore the possibility of a global minimum located elsewhere. Only the vicinity of the BSR is modified to make these test models from the best model obtained previously. For the Blake Ridge, one of the starting models is a wedge model, and three are LVZ models with different velocities and thicknesses (Figure 11). The starting models for the Carolina Rise are constructed similarly (Figure 12). The inversion procedure was repeated for each starting model, and the results are shown in Figures 11 and 12. Only a portion of the data around the BSR reflection was used to calculate the misfit, from 0.1 s prior to the reflection to the following 0.4 s, as the misfit of the remainder of the data is negligibly influenced by these changes in starting models. No improvement in misfit was achieved for either data set. Although this failure to find a better model with only a few different starting models does not confirm that our best model corresponds to the global minimum, the results of these test runs suggest that the major features of the best fit models are robust.

It is difficult to estimate uncertainty in the best fit model; the number of model parameters is large (>150), and each parameter probably has a different uncertainty. If a uniform uncertainty can be assumed for a small portion of model parameters, however, the uncertainty may be inferred by a random perturbation approach. For a given maximum velocity perturbation, 30 models were produced by randomly perturbing the 40 parameters around the BSR, and the mis-

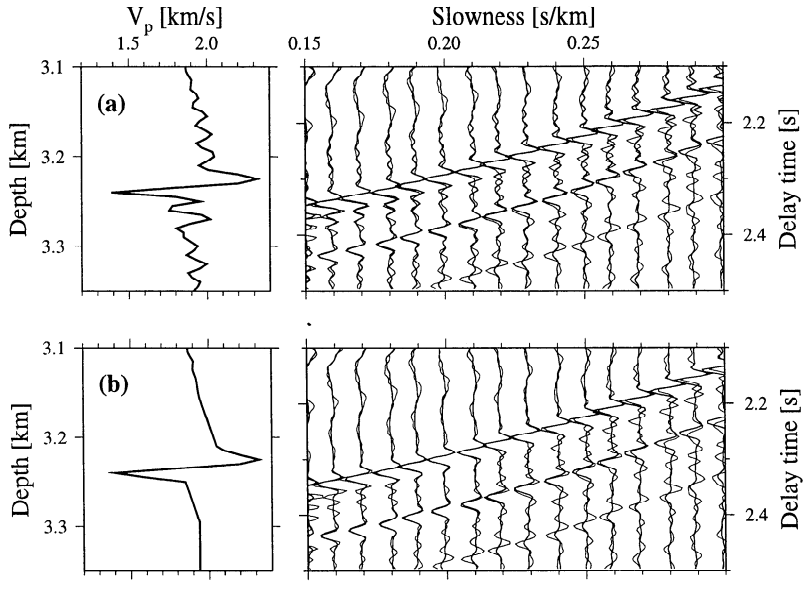

Figure 9. Synthetic seismograms are shown shown in thick line for (a) Blake Ridge best fit model, and (b) smoothed model. Observed wave field is also plotted in thin line for comparison. See text for discussion.

fit and the correlation factor between the resultant synthetics and the data were calculated for each random model, within the limited data portion of 0.5 s around the BSR as specified previously. The correlation factor is defined as $\sum D_i S_i / (\sum D_i^2 \sum S_i^2)^{1/2}$, where D_i and S_i are observed data and synthetic data, respectively [*Sen and Stoffa*, 1991], and it varies between 0 and 1. Figure 13 shows the normalized misfit relative to the misfit of the best fit model and the correlation factor as functions of maximum velocity perturbation for the case of the Blake Ridge data. The average misfit increases by 20% for 0.10 km/s perturbation and by 50% for 0.16 km/s perturbation. The average correlation factor is ~0.6 for 0.10 km/s perturbation and ~0.5 for 0.16 km/s perturbation. It is noted that the scatter in the correlation factors for a given velocity perturbation rapidly increases as the perturbation increases; around half of the random models have correlation factors lower than 0.5 for velocity perturbations larger than 0.10 km/s. Based on these two statistical quantities, we choose 0.10 km/s as a reasonable error bound for the P wave velocity models of the Blake Ridge and Carolina Rise BSRs.

We also investigated the model sensitivity to perturbations of other elastic parameters. Though densities and S wave velocities are hardly influenced by the possible existence of a small percentage of free gas (<10% saturation) beneath the BSR, the hydrates above the BSR may increase the S wave velocities by replacing pore fluid with hydrate crystals. The empirical relation of *Castagna et al.* [1985] for mudstone sediments produced a Poisson ratio of ~0.475 above the BSR, which may be too high for the hydrated region, though S wave velocities of hydrated sediments are poorly known. In order to estimate a possible impact of increased S wave velocities to the Blake Ridge result, a Poisson ratio of 0.40 was used for the possibly hydrated region above the BSR to calculate an alternative S wave velocity model from the best P wave velocity model. The inversion step was repeated with this S wave velocity model, and a similar short-wavelength variation resulted with slightly higher P wave velocity (~2.4 km/s) immediately above the BSR. Different sediment Q values were also tested, and a difference of ± 100 in Q_p resulted in ∓ 0.1 km/s in the maximum amplitude of the P wave velocity variation. Therefore the dominant features in the waveform inversion results, such as seen in the smoothed velocity model (Figure 9b), are well above the estimated error bounds.

Reflectivity Analysis

Although it is not commonly seen on other continental margins, "amplitude blanking" above the BSR is often quite intense on the Blake Ridge (Figure 2a) and has been attributed to hydrated sediments [e.g., *Dillon et al.*, 1980]. In addition, possible presence of free gas beneath the BSR, especially the thickness of a free gas zone, has been modeled based on the reflection coefficients of BSRs [e.g., *Miller et al.*, 1991]. In order to explore possible correlation between the reflectivity information provided by SCS data and the velocity structure estimated previously, reflection coefficients are calculated using the SCS data corresponding to the regions modeled by the waveform inversion. After a spherical divergence correction of $t^{1.0}$ is applied to the data, the seafloor reflection coefficient is first calculated as [*White*, 1977; *Warner*, 1990]

$$R_{sf} = \frac{A_m}{A_p} \tag{16}$$

where A_p and A_m are the maximum absolute amplitudes of the seafloor primary and multiple, respectively. The samplewise reflection coefficients R_i are then calculated referring to the seafloor primary as

$$R_i = \frac{A_i}{A_p} R_{sf} \tag{17}$$

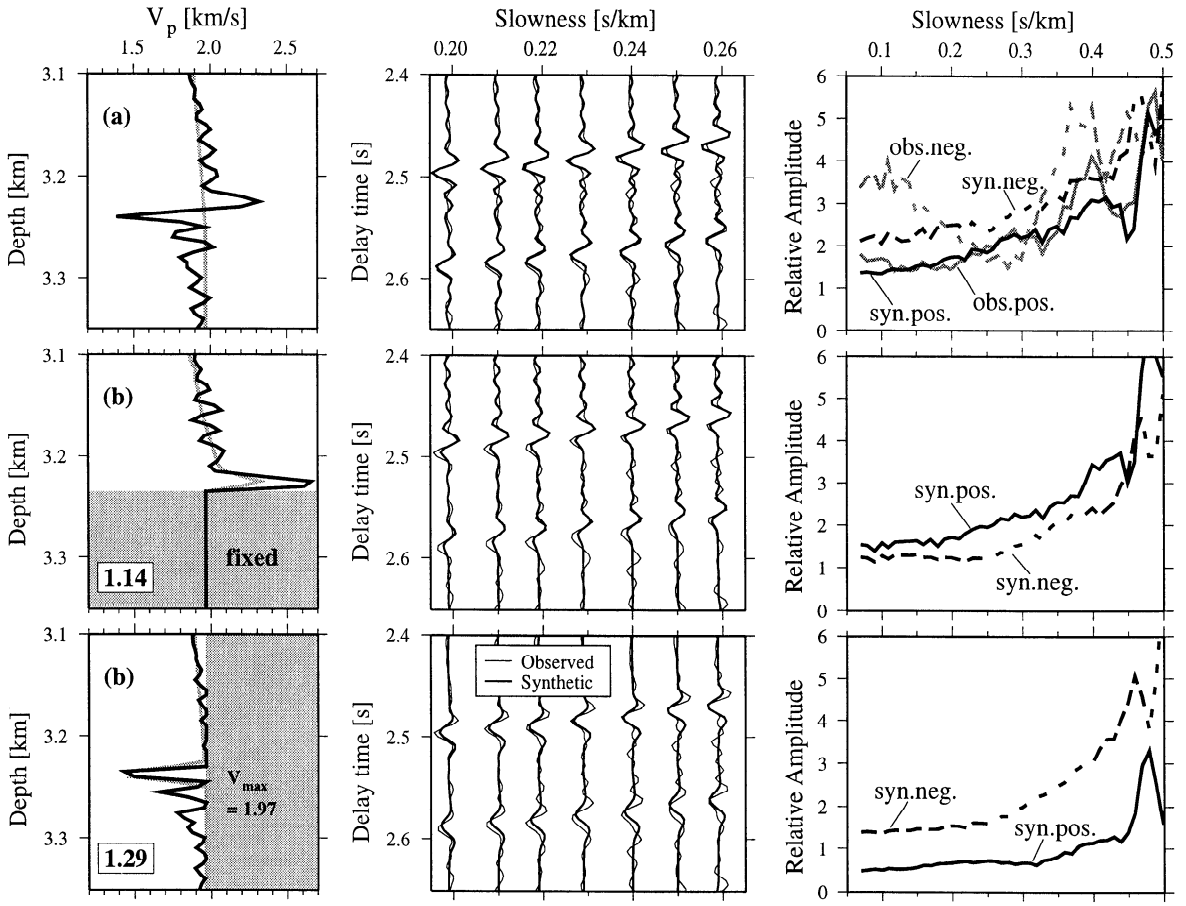

Figure 10. Results of Blake Ridge waveform inversion with additional constraints. (left) The final velocity model is shown in solid line, and the starting model is in gray. (middle) Synthetic seismograms corresponding to the final model are plotted in thick line, and the data are in thin line. (right) The relative amplitudes are plotted as a function of slowness. Solid line denotes the maximum positive amplitude of the synthetic BSR phase, and dashed line denotes the maximum negative amplitude. The sign of the maximum negative amplitude is reversed for direct comparison with the positive one. (a) The best fit model same as in Figure 9a. The relative amplitudes of the data are also shown in gray. (b) The best fit wedge-only model. The fixed portion is shaded. (c) The best fit LVZ-only model. The forbidden velocity space (> 1.97 km/s) is shaded. The misfit normalized by the misfit of the best fit model is also shown for Figures 10b and 10c.

where A_i is the absolute amplitude of the ith sample. Log-scale reflection coefficients or reflectance may be more suitable to interpret widely varying reflectivity such as amplitude blanking, and the reflectance γ_i may be defined as [*Lee et al.*, 1994]

$$\gamma_i = 20 \log_{10}(\frac{R_i}{R_0}) \qquad (18)$$

where R_0 is an arbitrary reference factor. R_0 of 0.4 is used here so a reflectance of -6.02 dB corresponds to a reflection coefficient of 0.2.

Nearly 30 SCS traces, which correspond to 1-km-wide bottoming points at BSR, were used for each site, and the results were summarized by taking maximum reflectance at every sample (Figure 14) because simple averaging can produce too low reflectance for dipping reflectors such as seen below the Blake Ridge BSR. Line 50 (Carolina Rise) shows overall higher reflectivity than line 31 (Blake Ridge), including seafloor and BSR reflections. Relative changes in reflectivity across the BSRs can serve as a quantitative measure of the blanking effect. While no significant change is seen for line 50, line 31 shows a blanked zone with low reflectance (3.90-4.25 s) above the BSR followed by a highly reflective zone (4.25-4.40 s). The Blake Ridge reflectance below 4.5 s is, however, as low as in the blanked zone, so it might be suitable to interpret the zone beneath the BSR up to 4.5 s as an "enhanced zone" rather than to interpret the zone above the BSR as a blanked zone.

Discussion

Comparison With Previous Work

Since the first direct indication of gas hydrates in deep-sea sediments on the Blake Ridge [*Ewing and Hollister*, 1972], a number of workers have investigated the nature of the hydrates stored in the ridge sediments using various seismic techniques as well as deep-sea drilling. The mapping of BSRs using single-channel and multichannel seismic profiling has been conducted extensively over the ridge, and the

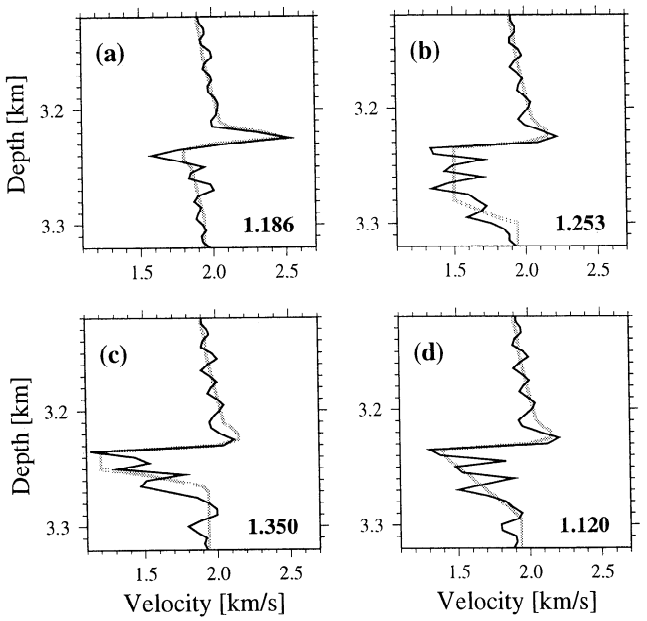

Figure 11. Starting (dashed line) and final (solid line) velocity models for Blake Ridge data. The starting models were derived from the velocity model of Figure 8a by replacing 20 layers in the vicinity of the BSR with (a) a high-velocity wedge above the BSR with a maximum of 2.5 km/s; (b) a 50-m-thick low-velocity zone below the BSR with 1.5 km/s; (c) a 20-m-thick low-velocity zone below the BSR with 1.2 km/s; and (d) a 60-m-thick, gradient low-velocity zone below the BSR with 1.4 km/s. The numbers beside the velocity models are the ratio of the final misfit to the original final misfit.

correlation with structural variation and sedimentary strata has indicated hydrated layers acting as gas traps and possible free gas migration along sedimentary strata [*Tucholke et al.*, 1977; *Dillon et al.*, 1980; *Paull and Dillon*, 1981; *Dillon et al.*, 1993].

Interval velocity analyses with multichannel seismic (MCS) data have commonly shown an anomalously high-velocity (2.1-2.4 km/s), thick (100-300 m) layer above the BSR [*Dillon and Paull*, 1983; *Rowe and Gettrust*, 1993]. An exception is the study by *Wood et al.* [1994], in which interval velocities do not exceed 2.0 km/s in the hydrate stability zone. The anomalously high-velocity zone is not consistent with the results of the wide-angle travel time inversions conducted in this study and by *Katzman et al.* [1994], which indicate that the lower half of the stability zone has a velocity of ~1.9 km/s. Since each velocity analysis represents a different location on the Blake Ridge, the inconsistency among these results may simply reflect regional variability. It should be noted, however, that the reliability of travel time analysis mainly depends on the aperture of data. The seafloor where strong BSRs are observed is usually as deep as ~3 km on the Blake Ridge, so a common-midpoint gather acquired by 3.6 km surface-tow streamer [*Dillon and Paull*, 1983] provides incident angles to the BSR with a range of only 25° if the BSR is located 500 m beneath the seafloor. *Rowe and Gettrust* [1993] used deep-tow MCS profiling system floating 350 m above the seafloor, which can only offer similarly limited angles (up to 20° at BSR) because of their short streamer (~600 m). The MCS data used by *Wood et al.* [1994] were acquired by a 6.0 km streamer with an accordingly larger maximum incident angle (~40°), and the wide-angle reflection data recorded by OBHs can provide an incident angle as large as ~60° for 6-km offset. It is also noted that interval velocity estimates using closely spaced reflections tend to result in high ambiguities [e.g., *Wood et al.*, 1994], and therefore it is preferable to estimate high-resolution velocity structure from waveforms rather than from travel times.

Bottom simulating reflectors often show significant lateral variation, and their reflection coefficients and waveforms at vertical incidence have been analyzed to model possible free gas zones beneath BSRs [*White*, 1977; *Miller et al.*, 1991; *Lee et al.*, 1994; *Katzman et al.*, 1994]. These studies have indicated that if the gas layer has a sharp bottom, destructive and constructive interference or the "tuning effect" [*Widess*, 1973] has a dominant control on the seismic appearance of BSR. Our reflectivity analysis suggests another complicating factor: the Carolina Rise BSR has a higher reflection coefficient than the Blake Ridge BSR (Figure 14), whereas the waveform inversion results show a much larger impedance contrast at the Blake Ridge BSR (Figure 8). The tuning effect including both a hydrate wedge and a free gas layer can produce various reflection coefficients with different wedge shapes and different gas layer thickness, and it is probably impractical to unambiguously infer realistic velocity structure around the BSR only from reflection coefficients when a hydrate wedge is probable.

Although the above ambiguity seems to be circumvented by AVO analysis, which utilizes a wide range of incidence [e.g., *Minshull and White*, 1989], AVO analysis explores

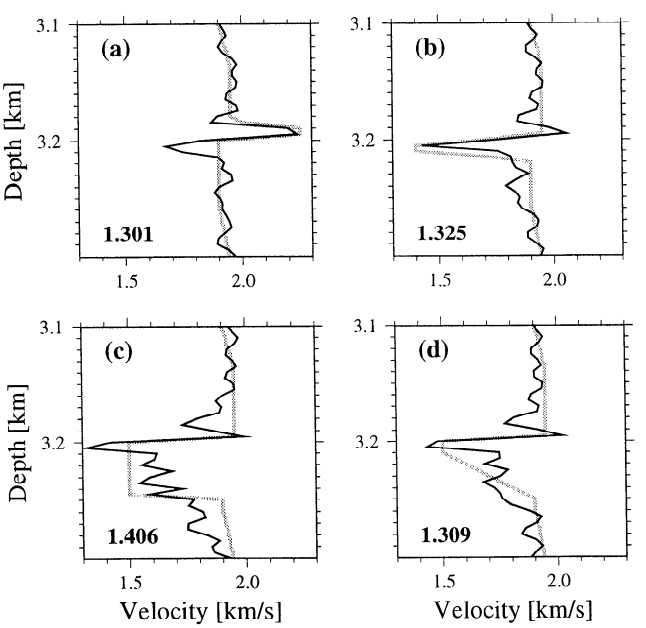

Figure 12. Starting (dashed line) and final (solid line) velocity models for Carolina Rise data. The starting models were derived from the velocity model of Figure 8b by replacing 20 layers in the vicinity of the BSR with (a) a high-velocity wedge above the BSR with a maximum of 2.25 km/s; (b) a 20-m-thick low-velocity zone below the BSR with 1.4 km/s; (c) a 50-m-thick low-velocity zone below the BSR with 1.5 km/s; and (d) a 50-m-thick, gradational low-velocity zone below the BSR with a minimum of 1.5 km/s.

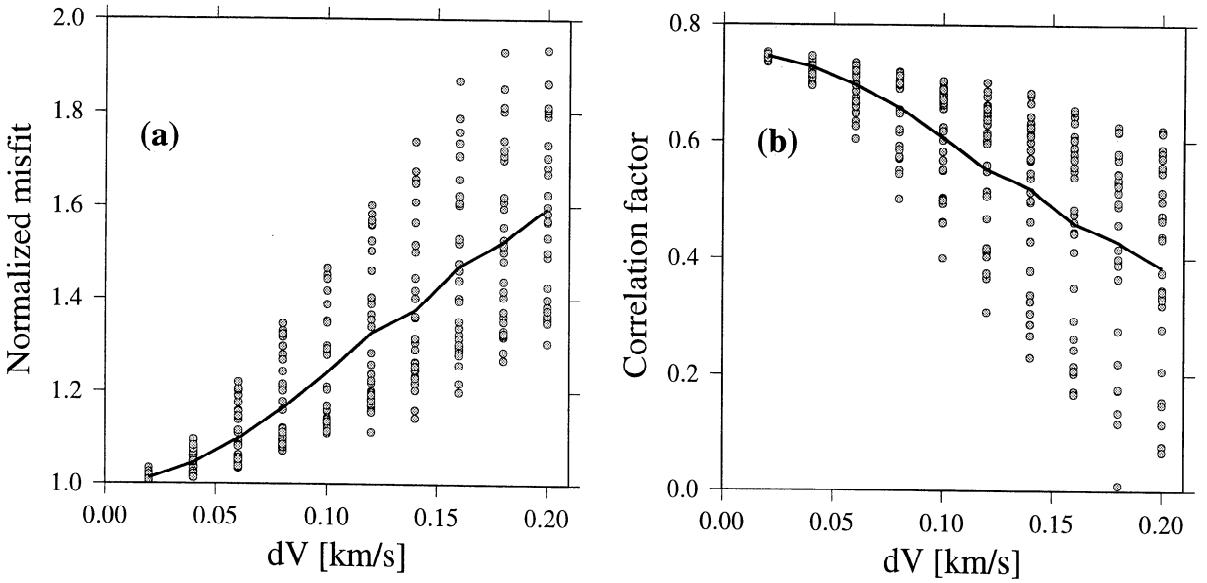

Figure 13. Example of uncertainty estimation for waveform inversion results (showing the case of Blake Ridge). (a) The misfit normalized by the misfit of the best fit model and (b) the correlation factor as functions of velocity perturbation. Solid line denotes an average of the results of 30 random models.

only a prescribed solution space, so that the best model that can reproduce well the observed AVO behavior may be far from the true model, as clearly demonstrated by debates on the existence of a free gas zone beneath the Cascadia margin BSR [*Hyndman and Spence*, 1992; *Singh et al.*, 1993; *MacKay et al.*, 1994]. *Katzman et al.* [1994] investigated two candidate models, i.e., hydrate wedge model and free gas model, with AVO analysis, and they rejected the hydrate wedge model for the Blake Ridge data. As shown by this study, however, the Blake Ridge data are best explained by the combination of both models. Though we could expand the limited solution space to some extent by preparing a number of different candidate models [*Andreassen et al.*, 1995], the AVO analysis is sometimes unable to discriminate between different models that produce similar AVO character, because amplitude data other than peak amplitudes are neglected in the AVO comparison. On the other hand, waveform inversion explores a virtually infinite solution space using all data samples; thus we were able to confidently derive the high-resolution velocity model in a more objective and automated way.

Possible Hydrate Distribution

It is not straightforward to calculate possible amount of hydrates in sediments from seismic velocity information. How hydrates are actually distributed in sediments and how they modify the sediment bulk moduli are poorly known. If hydrates simply form in the sedimentary pore space, the velocity of the hydrated sediment, V_p, may be approximated by the following three-phase, time-average equation [*Pearson et al.*, 1983]:

$$\frac{1}{V_p} = \frac{\phi(1-S)}{V_w} + \frac{\phi S}{V_h} + \frac{(1-\phi)}{V_m} \qquad (19)$$

where V_w, V_m, and V_h are the velocities of water, matrix, and pure hydrate, respectively; ϕ is porosity; and S is the concentration of hydrate in the pore space. Equation (19) can be rewritten with the velocity of the unhydrated sediment, V_u, and the bulk volume concentration of hydrate, C, as follows:

$$C = \left(\frac{1}{V_p} - \frac{1}{V_u}\right)\Big/\left(\frac{1}{V_h} - \frac{1}{V_w}\right) \qquad (20)$$

so hydrate concentration can be estimated if a reasonable estimate of the unhydrated sediment velocity is available.

Regardless of the strong variation in BSR appearance, no significant lateral variation in the average velocity was detected by 2-D travel time inversion for the Blake Ridge [*Katzman et al.*, 1994], which suggests that sediments over the entire surveyed portion of the Blake Ridge contain a similar amount of hydrate and that V_u cannot be resolved from the travel time inversion results. *Wood et al.* [1994] suggested that the unhydrated sediment on the Blake Ridge may have a velocity of 1.8-1.9 km/s at 0.35 to 0.45 km subbottom depth, by extrapolating the velocity profile from near the seafloor where no hydrate is usually expected. Assuming that V_u is 1.85 km/s and V_h is 3.3 km/s, an average hydrate concentration of ~3% of total sediment volume is expected for the ~200 m thick layer above the Blake Ridge BSR. On the Carolina Rise, the upper 200 m of the sediment column has a higher velocity (1.65-1.68 km/s) than that on the Blake Ridge (1.58 km/s), so V_u around the depth of the BSR may also be higher. Thus the average velocity of 1.87 km/s for the lower half of the hydrate stability zone hardly requires a notable amount of hydrate, and the average hydrate concentration is probably very small (<1%). Accurate estimation of C is difficult because of the uncertainty both in V_u and V_p, and equation (19) may not be valid under several conditions (see summary by *Lee et al.* [1993]), so the estimates attempted in this section should be considered crude approximations. Nevertheless, the results of the travel time inversion indicate that bulk hydrate concentration in the Blake Ridge sediments must be higher than that in the Carolina Rise sediments regardless of the uncertainties in absolute concentrations.

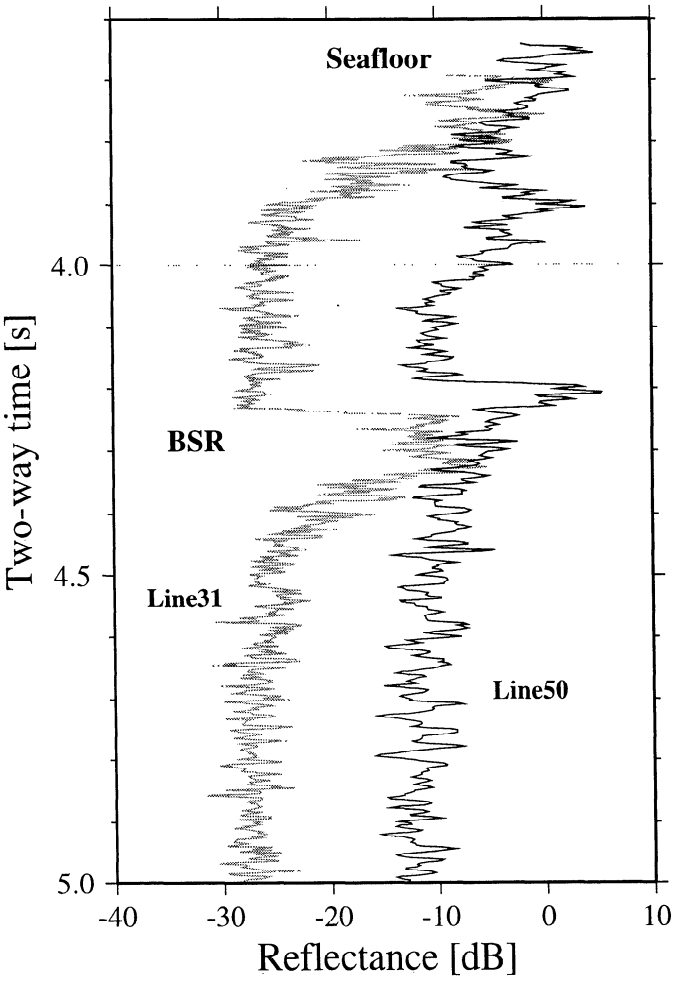

Figure 14. Reflectance profiles for line 31 (Blake Ridge, gray line) and for line 50 (Carolina Rise, solid line). Overall higher reflectivities on Carolina Rise are observed including seafloor and BSR reflections.

How hydrates are vertically distributed in the stability zone can be inferred from the short wavelength velocity variation. For the Blake Ridge BSR, the highest velocity increase (~0.35 km/s) is observed in a 15-m-thick zone just above the BSR, and the positive deviation from the background velocity diminishes around 100 m above the BSR. Thus the hydrates seem to be concentrated near the base of the stability zone, and the maximum concentration can be as high as ~20%. Our interpretation is substantiated by preliminary results of Ocean Drilling Program (ODP) Leg 164, which show anomalously low chloride contents just above the Blake Ridge BSR [*Ocean Drilling Program Leg 164 Shipboard Scientific Party*, 1996]. Though its magnitude is much smaller (~0.1 km/s), the velocity peak just above the BSR is also seen on the Carolina Rise, which implies a maximum hydrate concentration of ~7% at the base of the stability zone.

Based on the hypothesis that the weak reflectivities seen above BSRs are caused by hydrate cementation [*Dillon et al.*, 1980], *Lee et al.* [1993] proposed that amplitude information, if calibrated by velocity information, can also be used to estimate bulk hydrate concentration. At first glance, the reflectivities seem to correlate well with the hydrate concentrations estimated herein; more hydrates can be expected for the Blake Ridge, which shows significantly lower reflectivity above the BSR. However, the calculation of hydrate concentration using the blanking effect requires the accurate measurement of background reflectivity, which might be very low at the Blake Ridge. Based on vertical seismic profiling on ODP Leg 164, *Holbrook et al.* [1996] showed that the Blake Ridge BSR is underlain by a free gas zone with a thickness of at least 250 m and that the so-called blanked zone corresponds to an anomalously uniform sediment column accentuated by the subsequent highly reflective gas-bearing sediments, supporting the enhanced-zone interpretation.

Hydrate Formation by in situ Biogenic Activity

The primary source for natural gas hydrates has been thought to be biogenic methane, though the significance of thermogenic methane has been suggested by several authors (see discussion by *Minshull et al.* [1994]). There are three important parameters that control in situ hydrate formation: (1) the amount of organic carbon in sediments, (2) the efficiency of biogenic methane production, and (3) the methane solubility in pore fluid. The sediment cores from Deep Sea Drilling Project (DSDP) Leg 76 on the Blake Ridge are moderately rich in organic carbon (0.5-1.0%) [*Sheridan and Gradstein*, 1983]. Common organic concentrations in

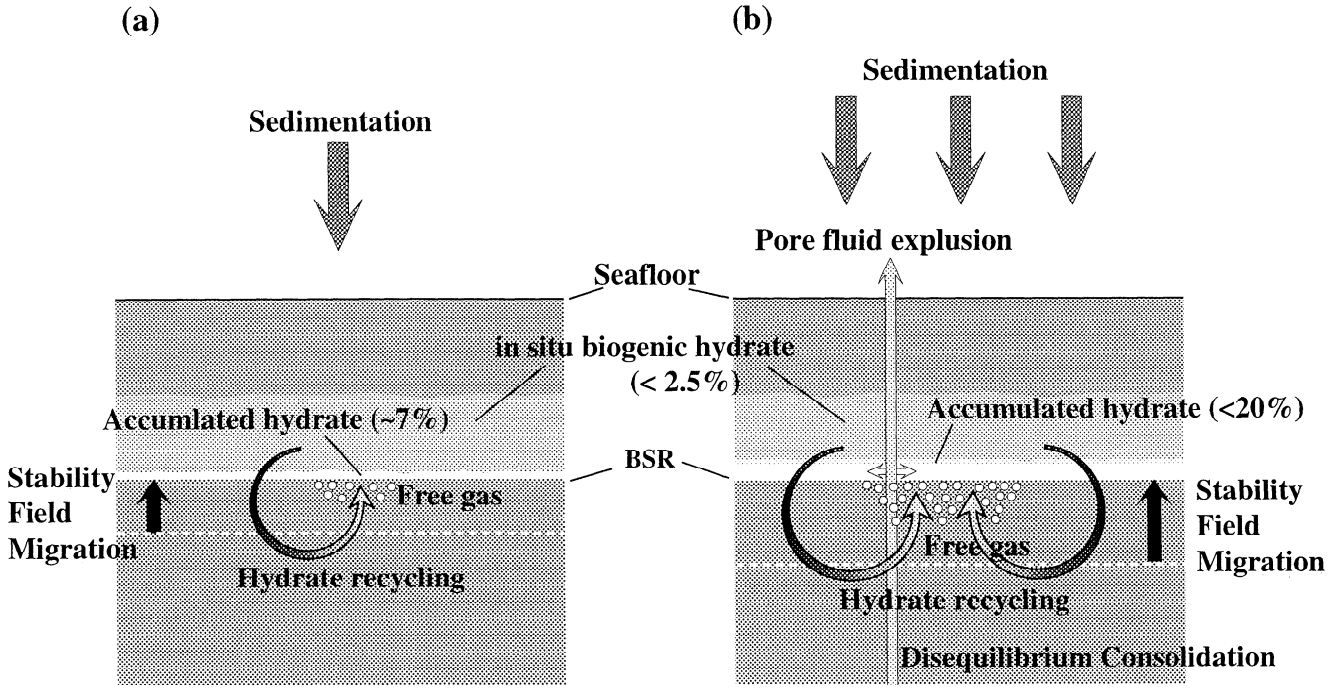

Figure 15. Schematic diagrams illustrating possible hydrate formation on passive margins in (a) normal depositional regime (e.g., Carolina Rise) and (b) rapid depositional regime (e.g., Blake Ridge). Weakly distributed biogenic hydrates (<2.5% concentration) are accumulated at the base of the hydrate stability field as the stability field migrates upward due to sedimentation. In the rapid depositional regime (Figure 15b), methane removed from rising fluid can further enhance the accumulation.

turbidite and hemipelagic sediments are also 0.5-1.0%, so a similar concentration can be expected on the Carolina Rise. For a 50% porosity sediment, the above range of organic concentration can produce as much as 1200 to 2400 mmol/L of hydrates if complete conversion occurs. Realistic efficiency, however, seems to be very small; proposed estimates range from less than 2% [*Claypool and Kaplan*, 1974] to ~20% [*Brooks et al.*, 1987]. For a hydrate to be formed, the amount of methane needs to exceed the solubility of methane in water [e.g., *Sloan*, 1990], though some authors argue that subsaturation hydrate formation is possible [e.g., *Handa*, 1990]. The solubility of methane in water is also not a well-known quantity. At pressures and temperatures corresponding to near the base of the stability zone in the surveyed area, the solubility is probably ~200 mmol/L [*Culberson and McKetta*, 1951; *Duan et al.*, 1992], and a theoretical study predicts a gradual increase in solubility as subseafloor depth increases [*Bishnoi et al.*, 1989]. In contrast, a sharp drop in the solubility by a factor of 3 to 5 across the gas-hydrate phase boundary has been reported by *Makogon et al.* [1972] though it violates the Gibbs phase rule. *Hyndman and Davis* [1992] suggested that sediment grain surface effects can result in such an apparent discontinuous decrease, and thus the effective solubility in the stability zone could be as low as ~70 mmol/L.

With 2% conversion rate, only 24-48 mmol/L of methane is produced from 0.5-1.0% organic carbon, which is below the saturation level even with the lowest estimate of the solubility. Since we have strong evidence for free gas trapped beneath the BSRs, it seems necessary to require somewhat higher efficiency in conversion. With the estimated maximum efficiency of ~20%, ~480 mmol/L of methane is produced from 1% organic carbon. Assuming that the solubility is 70 mmol/L, 410 mmol/L of methane is available to form gas hydrates. one mole of pure hydrate has a volume of ~0.12 L so that ~0.05 L of hydrate is formed from the above methane, replacing 5% of pore fluid. Thus the in situ biogenic hydrate formation can produce only 2.5% hydrate of total sediment volume at most, which is insufficient to explain the observed high-velocity spikes above the BSRs. This discrepancy seems to exceed the uncertainty inherent in the estimation using the seismic velocities, and some mechanism by which hydrates are accumulated at the base of the stability zone is obviously needed.

Mechanisms for Hydrate Accumulation

One possible mechanism is hydrate recycling caused by the migration of the stability zone [e.g., *Kvenvolden*, 1993; *Paull et al.*, 1994]. As sedimentation continues on the seafloor and the underlying sediments subside by compaction, the base of the stability zone migrates upward to follow a new pressure and temperature condition. If some hydrates are already present, they will dissociate into free gas as they are passed by the migrating phase boundary. Because of its buoyancy, the resultant free gas can migrate upward separately from pore fluid phase and form gas hydrates it reenters the hydrate stability zone (Figure 15). The concentration of hydrates formed by this mechanism is mainly controlled by sedimentation rate.

The Blake Ridge is a deep-sea, sediment-drift deposit [*Dillon and Popenoe*, 1988] with rapid sedimentation, and the sedimentation rates based on the DSDP Site 533 results

are 8 cm/kyr for Holocene-Pleistocene and 17 cm/kyr for Pliocene [*Sheridan and Gradstein*, 1983]. Since no drilling has been conducted on the Carolina Rise, which consists of continental slope sediments, we estimated its sedimentation rate using the sediment thicknesses determined by seismic studies [*Mountain and Tucholke*, 1985] as 2 cm/kyr (upper Pliocene-Present) and 5 cm/kyr (middle Miocene-upper Pliocene). The Blake Ridge sediment rates estimated by the same method are 4 cm/kyr (upper Pliocene-Present) and 11 cm/kyr (middle Miocene-upper Pliocene), indicating possible errors in this approach. As a robust estimate, therefore, we conclude that the sedimentation rate on the Blake Ridge has been more than twice as fast as that on the Carolina Rise at least for the past 10 Myr. Assuming a sedimentation rate of 5 cm/kyr, a 15-m-thick, 20% hydrate layer can be produced within 20 kyr from average 3% hydrate concentration (within 60 kyr for 1% hydrate concentration) if dissociated free gas completely returns into the stability zone. The migration of free gas depends on its bubble size and the permeability of the sediment. If the buoyancy of gas bubble is not sufficient to overcome its surface tension, it would move downward with the pore fluid rather than ascend through it [e.g., *Gunstensen and Rothman*, 1993]. Some sedimentary strata may act as an impermeable barrier, and gas migration paths may be restricted along fissures and faults breaking through the barrier [*Rowe and Gettrust*, 1993; *Dillon et al.*, 1993]. In addition to these possibilities for reduced efficiency in hydrate recycling, the continuous condensation process can be frequently disrupted by pressure drops that may result from local sediment slumps or global sea level change due to glaciation. Nevertheless, it seems likely that the hydrate recycling mechanism explains some portion of the inferred high concentration of hydrates at the base of the stability zone.

Another possibility is methane removal from upward fluid expulsion [*Hyndman and Davis*, 1992]. As emphasized by *Hyndman and Davis* [1992], there is no upward fluid expulsion for a normal depositional regime [e.g., *Einsele*, 1977]. Disequilibrium consolidation caused by rapid deposition is required to expel the pore fluid out of the downgoing sediment matrices. The Pliocene sedimentation rate on the Blake Ridge was much higher (~17 cm/kyr) than at present, so the transition from high-porosity sediments to relatively low-porosity sediments may have resulted in fluid expulsion through the seafloor. The quantity of the expelled fluid reaches 100 m^3/m^2 if average porosity decreases by 5% over 2-km-thick sediments, and a 15-m-thick, 8% hydrate layer can be formed if the methane removal efficiency is 50 mmol/L. Since the difference in the expected amounts of hydrate concentration between the Blake Ridge and the Carolina Rise is not easily explained by the difference in the sedimentation rates only, this additional concentration mechanism may have further enhanced the hydrate accumulation on the Blake Ridge (Figure 15b).

One may expect that possible fluid expulsion, if in progress, might heighten the heat flow on the Blake Ridge relative to that on the Carolina Rise, though no significant difference between the two sites has been recognized [*Ruppel et al.*, 1995]. Even if the above 5% porosity change occurs within 1.0 Myr and still continues to the present, the fluid migration rate would be only $\sim 3 \times 10^{-12}$ m/s so that its effect on heat flow is too small to be observable ($\ll 1$ mW/m^2) [*Bredehoeft and Papadopulos*, 1965].

Conclusion

Joint travel time inversion with wide-angle and vertical-incidence data was performed to estimate the 2-D average velocity model of the Carolina Rise. The comparison with the Blake Ridge 2-D velocity model from the previous study clearly shows that the 200-m-thick layer beneath the seafloor on the Carolina Rise has higher sediment velocities (>1.65 km/s) than that on the Blake Ridge (1.58 km/s). The second layer, which occupies the lower half of the stability zone, however, shows very similar velocities (1.87 and 1.89 km/s) at the two sites. If the difference in the velocities of the first layer indicates higher background velocities on the Carolina Rise, the similarity seen for the second layer implies a somewhat higher degree of hydrate concentration on the Blake Ridge.

Using full waveform inversion, we successfully derived high-resolution velocity models from nearly one-dimensional OBH wide-angle data sets on the Blake Ridge and the Carolina Rise. The obtained waveform fits are good, and the best fit model for the Blake Ridge data consists of a high-velocity wedge above the BSR and a low-velocity zone below the BSR. The highest-velocity peak has a thickness of ~15 m and reaches ~2.3 km/s just above the BSR, indicating densely concentrated hydrates at the base of the stability zone. On the other hand, the Carolina Rise data are best explained by a model with a similar low-velocity layer beneath the BSR and a much smaller high-velocity peak above the BSR (~2.0 km/s). The low velocities beneath the BSRs (~1.4 km/s) probably reflect the presence of free gas with low saturation (<10%).

Reflectivities were also calculated using the SCS data, and the Carolina Rise shows higher reflectivities than the Blake Ridge overall. The relative changes in reflectivity were used to evaluate amplitude blanking above the BSR. Although very weak reflectivity is observed above the Blake Ridge BSR, it may originate in a similarly weak background reflectivity. The waveform inversion result for the Blake Ridge suggests that, conversely, the reflectivity of the sedimentary strata below the BSR may be enhanced by trapped free gas.

The amounts of hydrates were estimated based on these velocity models, and the lower half of the stability zone on the Blake Ridge may have a hydrate concentration of ~3% total sediment volume on average, whereas hydrate on the Carolina Rise is barely detectable. The fine-scale structure of hydrate distribution was also inferred from the short-wavelength variation above the BSRs. The hydrates seem to be highly concentrated at the base of the stability field both on the Blake Ridge and the Carolina Rise, though the maximum concentration estimated on the Blake Ridge (~20%) is much higher than that on the Carolina Rise (~7%). The in situ biogenic hydrate formation can produce only ~2.5% bulk hydrate concentration at most, so that some secondary accumulation mechanism is necessary to explain the high concentration. Hydrate recycling caused by stability field migration is the most probable mechanism, and upward fluid expulsion on the Blake Ridge may have provided an additional mechanism of concentration.

Acknowledgments. We gratefully acknowledge the captain and crew of the R/V *Cape Hatteras* for their cooperation. We thank Charlie Paull for his substantial role in motivating this study. We thank Tim Boynton for the SCS data acquisition; Mike Purdy, Beecher Wooding, and Ken Peal for the OBH data acquisition; and Dave DuBois, Don Koelsch, Jim Broda, and Walter Borowski for smooth shipboard operation. Dave DuBois and Jim Dolan assisted with OBH data processing. We thank Debbie Hutchinson, Bill Dillon, Uri ten Brink, and Ingo Pecher for illuminating discussions during this work. J.K. thanks Tricia Murray, Dave Lyness, and Paula Aarons for their hospitality during his stay in Cambridge. Dan Lizarralde, Rafi Katzman, John Collins, and Graham Kent were always helpful for constructive discussion. We appreciate Dan Lizarralde, Walter Borowski, Peter Kelemen, George Spence, Warren Wood, and a JGR Associate Editor for careful reviews of the manuscript, and Lois Gast for editorial assistance during revision. Most of figures were prepared with the GMT system [*Wessel and Smith*, 1991]. J.K. was supported partly by the Ishizaka Foundation scholarship. This work was supported by NSF grants OCE-9101887 and OCE-9302477. Woods Hole Oceanographic Institution contribution 9452 and University of Cambridge (Department of Earth Sciences) contribution 4931.

References

Andreassen, K., P. E. Hart, and A. Grantz, Seismic studies of a bottom simulating reflection related to gas hydrate beneath the continental margin of the Beaufort Sea, *J. Geophys. Res.*, *100*, 12659–12673, 1995.

Bishnoi, P. R., A. K. Gupta, P. Englezos, and N. Kalogerakis, Multiphase equilibrium flash calculations for systems containing gas hydrates, *Fluid Phase Equilibria*, *53*, 97–104, 1989.

Bredehoeft, J. D., and I. S. Papadopulos, Rates of vertical groundwater movement estimated from the Earth's thermal profile, *Water Resour. Res.*, *1*, 325–328, 1965.

Brooks, J., C. Cornford, and R. Archer, The role of hydrocarbon source rocks in petroleum exploration, *Geol. Soc. Spec. Publ.*, *26*, 17–46, 1987.

Castagna, J. P., M. L. Batzle, and R. L. Eastwood, Relationship between compressional-wave and shear-wave velocities in clastic silicate rocks, *Geophysics*, *50*, 571–581, 1985.

Chapman, C. H., Generalized radon transfroms and slant stacks, *Geophys. J. R. Astron. Soc.*, *66*, 445–453, 1981.

Chapman, C. H., and J. A. Orcutt, The computation of body wave synthetic seismograms in laterally homogeneous media, *Rev. Geophys.*, *23*, 105–163, 1985.

Claypool, G. E., and I. R. Kaplan, The origin and distribution of methane in marine sediments, in *Natural Gases in Marine Sediments*, edited by I. R. Kaplan, pp. 99–139, Plenum, New York, 1974.

Culberson, O. L., and J. J. McKetta, Phase equilibria in hydrocarbon systems III — The solubility of methan in water at pressures to 10,000 PSIA, *Trans. AIME*, *192*, 223–226, 1951.

Dietrich, M., and F. Kormendi, Perturbation of the plane-wave reflectivity of a depth-dependent elastic medium by weak inhomogeneities, *Geophys. J. Int.*, *100*, 203–214, 1990.

Dillon, W. P., and C. K. Paull, Marine gas hydrates II, geophysical evidence, in *Natural Gas Hydrates: Properties, Occurrence, Recovery*, pp. 73–90, Butterworth, Boston, Mass., 1983.

Dillon, W. P., and P. Popenoe, The Blake Plateau Basin and Carolina Trough, in *The Geology of North America*, vol. I-2, *The Atlantic Continental Margin*, edited by R. E. Sheridan and J. A. Grow, pp. 291–328, Geol. Soc. of Am., Boulder, Colo., 1988.

Dillon, W. P., J. A. Grow, and C. K. Paull, Unconventional gas hydrate seals may trap gass off southeast U.S., *Oil Gas J.*, *78*, 124–130, 1980.

Dillon, W. P., M. W. Lee, K. Fehlhaber, and D. F. Coleman, Gas hydrates on the Atlantic Continental Margin of the United States — Controls on concentration, in *The Future of Energy Gases*, edited by D. G. Howell, pp. 313–330, U.S. Geol. Surv., Reston, Va., 1993.

Dobrynin, V. M., Y. P. Korotajev, and D. V. Plyuschev, Gas hydrate: a possible energy source, in *Long Term Energy Resources*, edited by R. G. Mayer and J. C. Olson, pp. 727–729, Pitman, London, 1981.

Domenico, S. N., Effect of brine-gas mixture on velocity in an unconsolidated sand reservoir, *Geophysics*, *41*, 882–894, 1976.

Duan, Z., N. Møller, J. Greenberg, and J. H. Weare, The prediction of methane solubility in natural waters to high ionic strength from 0 to 250°C and from 0 to 1600 bar, *Geochim. Cosmochim. Acta*, *56*, 1451–1460, 1992.

Einsele, G., Range, velocity and material flux of compaction flow in growing sedimentary sequences, *Sedimentology*, *24*, 639–655, 1977.

Ewing, J. I., and C. D. Hollister, Regional aspects of deep sea drilling in the western North Atlantic, *Initial Rep. Deep Sea Drill. Proj.*, *11*, 951–973, 1972.

Gunstensen, A. K., and D. H. Rothman, Lattice-Boltzmann studies of immiscible two-phase flow through porous media, *J. Geophys. Res.*, *98*, 6431–6441, 1993.

Hamilton, E. L., Sound velocity-density relations in sea-floor sediments and rocks, *J. Acoust. Soc. Am.*, *63*, 366–377, 1978.

Handa, Y. P., Effect of hydrostatic pressure and salinity on the stability of gas hydrates, *J. Phys. Chem.*, *94*, 2652–2657, 1990.

Harding, A. J., Slowness-time mapping of near offset seismic reflection data, *Geophys. J. R. Astron. Soc.*, *80*, 463–492, 1985.

Henry, M., J. A. Orcutt, and R. L. Parker, A new method for slant stacking refraction data, *Geophys. Res. Lett.*, *7*, 1073–1076, 1991.

Holbrook, W. S., H. Hoskins, W. T. Wood, R. A. Stephen, D. Lizarralde, and Leg 164 Science Party, Methane hydrate and free gas on the Blake Ridge from vertical seismic profiling, *Science*, *273*, 1840–1843, 1996.

Hyndman, R. D., and E. E. Davis, A mechanism for the formation of methane hydrate and seafloor bottom-simulating reflectors by vertical fluid explusion, *J. Geophys. Res.*, *97*, 7025–7041, 1992.

Hyndman, R. D., and G. D. Spence, A seismic study of methane hydrate marine bottom simulating reflectors, *J. Geophys. Res.*, *97*, 6683–6698, 1992.

Jannane, M., et al., Wavelengths of earth structures that can be resolved from seismic reflection data, *Geophysics*, *54*, 906–910, 1989.

Kappus, M. E., A. J. Harding, and J. A. Orcutt, A comparison of tau-*p* transform methods, *Geophysics*, *55*, 1202–1215, 1990.

Katzman, R., W. S. Holbrook, and C. K. Paull, Combined vertical-incidence and wide-angle seismic study of a gas hydrate zone, Blake Ridge, *J. Geophys. Res.*, *99*, 17975–17995, 1994.

Kennett, B. L. N., and N. J. Kerry, Seismic waves in a stratified half space, *Geophys. J. R. Astron. Soc.*, *57*, 557–583, 1979.

Kormendi, F., and M. Dietrich, Nonlinear waveform inversion of plane-wave seismograms in stratified elastic media, *Geophysics*, *56*, 664–674, 1991.

Kvenvolden, K. A., Methane hydrate — A major reservoir of carbon in the shallow geosphere, *Chem. Geol.*, *71*, 41–71, 1988a.

Kvenvolden, K. A., Methane hydrates and global climate, *Global Biogeochem. Cycles*, *2*, 221–229, 1988b.

Kvenvolden, K. A., Gas hydrates — Geological perspective and global change, *Rev. Geophys.*, *31*, 173–187, 1993.

Lee, M. W., D. R. Hutchinson, W. P. Dillon, J. J. Miller, W. F. Agena, and B. A. Swift, Method of estimating the amount of in situ gas hydrates in deep marine sediments, *Mar. Pet. Geol.*, *10*, 493–506, 1993.

Lee, M. W., D. R. Hutchinson, W. F. Agena, W. P. Dillon, J. J. Miller, and B. A. Swift, Seismic character of gas hydrates on the southeastern U.S. continental margin, *Mar. Geophys. Res.*, *16*, 163–184, 1994.

Leggett, J., The nature of the greenhouse threat, in *Global Warming, The Greenpeace Report*, pp. 14–43, Oxford Univ. Press, New York, 1990.

MacDonald, G. J., The future of methane as an energy resource, *Annu. Rev. Energy*, *15*, 53–83, 1990.

MacKay, M. E., R. D. Jarrard, G. K. Westbrook, R. D. Hyndman, and Shipboard Scientific Party of Ocean Drilling Program Leg 146, Origin of bottom-simulating reflectors: Geophysical evidence from the Cascadia accretionary prism, *Geology*, *22*, 459–462, 1994.

Makogon, Y. F., V. I. Tsarew, and N. V. Cherskiy, Formation of large natural gas fields in zones of permanently low temperatures, *Dokl. Akad. Nauk SSSR*, Engl. Transl., *205*, 215, 1972.

McIver, R. D., Gas hydrate, in *Long Term Energy Resources*, edited by R. G. Mayer and J. C. Olson, pp. 713–726, Pitman, London, 1981.

Miller, J. J., M. W. Lee, and R. von Huene, An analysis of a seismic reflection from the base of a gas hydrate zone, offshore Peru, *AAPG Bull.*, *75*, 910–924, 1991.

Minshull, T., and R. White, Sediment compaction and fluid migration in the Makran Accretionary Prism, *J. Geophys. Res.*, *94*, 7387–7402, 1989.

Minshull, T. A., and S. C. Singh, Shallow structure of oceanic crust in the western north Atlantic from seismic waveform inversion and modeling, *J. Geophys. Res.*, *98*, 1777–1792, 1993.

Minshull, T. A., S. C. Singh, and G. K. Westbrook, Seismic velocity structure at a gas hydrates reflector, offshore western Colombia, from full waveform inversion, *J. Geophys. Res.*, *99*, 4715–4734, 1994.

Mountain, G. S., and B. E. Tucholke, Mesozoic and Cenozoic geology of the U.S. Atlantic Continental Slope and Rise, in *Geologic Evolution of the United States Atlantic Margin*, edited by C. W. Poag, chap. 8, pp. 293–341, Van Nostrand Reinhold, New York, 1985.

Murphy, W. F., Acoustic measures of partial gas saturation in tight sandstones, *J. Geophys. Res.*, *89*, 11549–11559, 1984.

Nisbet, E. G., The end of the ice age, *Can. J. Earth. Sci.*, *27*, 148–157, 1990.

Ocean Drilling Program Leg 164 Shipboard Scientific Party, Methane gas hydrate drilled at Blake Ridge, *Eos Trans. AGU*, *77*, 219, 1996.

Ostrander, W. J., Plane-wave reflection coefficients for gas sands at nonnormal angles of incidence, *Geophysics*, *49*, 1637–1648, 1984.

Paull, C. K., and W. P. Dillon, Appearance and distribution of the gas hydrate reflection in the Blake Ridge region, offshore southeastern United States, *U.S. Geol. Surv. Misc. Field Stud. Map*, *MF-1252*, 1981.

Paull, C. K., W. Ussler III, and W. P. Dillon, Is the extent of glaciation limited by marine gas-hydrates?, *Geophys. Res. Lett.*, *18*, 432–434, 1991.

Paull, C. K., W. Ussler III, and W. S. Borowski, Sources of biogenic methane to form marine gas hydrates, *Ann. N. Y. Acad. Sci.*, *715*, 392–411, 1994.

Pearson, C. F., P. M. Halleck, P. L. McGulre, R. Hermes, and M. Mathews, Natural gas hydrate: A review of in situ properties, *J. Phys. Chem.*, *87*, 4180–4185, 1983.

Rowe, M. M., and J. F. Gettrust, Fine structure of methane hydrate-bearing sediments on the Blake Outer Ridge as determined from deep-tow multichannel seismic data, *J. Geophys. Res.*, *98*, 463–473, 1993.

Ruppel, C., R. P. Von Herzen, and A. Bonneville, Heat flux through an old (~175 Ma) passive margin: Offshore southeastern United States, *J. Geophys. Res.*, *100*, 20037–20057, 1995.

Schultz, P. S., and J. F. Claerbout, Velocity estimation and downward continuation by wavefront synthesis, *Geophysics*, *43*, 691–714, 1978.

Sen, M. K., and P. L. Stoffa, Nonlinear one-dimensional seismic waveform inversion using simulated annealing, *Geophysics*, *56*, 1624–1638, 1991.

Sheridan, R. B., and F. M. Gradstein, Site reports and underway data, *Initial Rep. Deep Sea Drill. Proj.*, *76*, 35–80, 1983.

Singh, S. C., G. F. West, and C. H. Champman, On plane-wave decomposition: Alias removal, *Geophysics*, *54*, 1339–1343, 1989.

Singh, S. C., T. A. Minshull, and G. D. Spence, Velocity structure of a gas hydrate reflector, *Science*, *260*, 204–207, 1993.

Sloan, E. D., *Clathrate Hydrates of Natural Gas*. Marcel Dekker, New York, 1990.

Tucholke, B. E., G. M. Bryan, and J. I. Ewing, Gas-hydrate horizons detected in seismic-profiler data from the western North Atlantic, *AAPG Bull.*, *61*, 698–707, 1977.

Warner, M., Absolute reflection coefficients from deep seismic reflections, *Tectonophysics*, *173*, 15–23, 1990.

Wessel, P., and W. H. F. Smith, Free software helps map and display data, *Eos Trans. AGU*, *72*, 441, 1991.

Whalley, E., Speed of longitudinal sound in clathrate hydrates, *J. Geophys. Res.*, *85*, 2539–2542, 1980.

White, R. S., Seismic bright spots in the Gulf of Oman, *Earth Planet. Sci. Lett.*, *37*, 29–37, 1977.

Widess, M. B., How thin is a thin bed?, *Geophysics*, *38*, 1176–1180, 1973.

Wood, W. T., P. L. Stoffa, and T. H. Shipley, Quantitative detection of methane hydrate through high-resolution seismic velocity analysis, *J. Geophys. Res.*, *99*, 9681–9695, 1994.

Zelt, C. A., and R. B. Smith, Seismic traveltime inversion for 2-D crustal velocity structure, *Geophys. J. Int.*, *108*, 16–34, 1992.

W. S. Holbrook and J. Korenaga, Woods Hole Oceanographic Institution, Woods Hole, MA 02543-1542. (e-mail:sholbrook@whoi.edu; korenaga@mit.edu)

T. A. Minshull and S. C. Singh, Bullard Laboratories, University of Cambridge, Cambridge, CB3 0EZ, England. (e-mail: minshull@esc.cam.au.uk; singh@esc.cam.ac.uk)

(Received April 8, 1996; revised February 25, 1997; accepted March 5, 1997.)